A&A 393, 461–483 (2002)
DOI: 10.1051/0004-6361:20021023

Astronomy & Astrophysics

The blue compact dwarf galaxy I Zw 18: A comparative study of its low-surface-brightness component

P. Papaderos[1], Y. I. Izotov[2], T. X. Thuan[3], K. G. Noeske[1], K. J. Fricke[1], N. G. Guseva[2], and R. F. Green[4]

[1] Universitäts–Sternwarte, Geismarlandstraße 11, 37083 Göttingen, Germany
[2] Main Astronomical Observatory, National Academy of Sciences of Ukraine, 27 Zabolotnoho str., 03680 Kyiv, Ukraine
[3] Astronomy Department, University of Virginia, Charlottesville, VA 22903, USA
[4] National Optical Astronomy Observatory, Tucson, AZ 85726, USA

Received 31 May 2002 / Accepted 9 July 2002

Abstract. Using *HST*⋆ and ground-based optical and NIR imaging data⋆⋆, ⋆⋆⋆, we investigate whether the blue compact dwarf (BCD) galaxy I Zw 18 possesses an extended low-surface-brightness (LSB) old stellar population underlying its star-forming regions, as is the case in the majority of BCDs. This question is central to the long-standing debate on the evolutionary state of I Zw 18. We show that the exponential intensity decrease observed in the filamentary LSB envelope of the BCD out to $\gtrsim$18″ ($\gtrsim$1.3 kpc assuming a distance of 15 Mpc) is not due to an evolved stellar disc underlying its star-forming regions, but rather, due to extended ionized gas emission. Ionized gas accounts for more than 80% of the line-of-sight emission at a galactocentric distance of ∼0.65 kpc (∼3 effective radii), and for $\gtrsim$30% to 50% of the *R* light of the main body of I Zw 18. Broad-band images reveal, after subtraction of nebular line emission, a relatively smooth stellar host extending slightly beyond the star-forming regions. This unresolved stellar component, though very compact, is not exceptional for intrinsically faint dwarfs with respect to its structural properties. However, being blue over a radius range of ∼5 exponential scale lengths and showing little colour contrast to the star-forming regions, it differs strikingly from the red LSB host of standard BCDs. This fact, together with the comparably blue colours of the faint C component, ∼1.6 kpc away from the main body of I Zw 18, suggests that the formation of I Zw 18 as a whole has occurred within the last 0.5 Gyr, making it a young BCD candidate. Furthermore, we show that the ionized envelope of I Zw 18 is not exceptional among star-forming dwarf galaxies, neither by its exponential intensity fall-off nor by its scale length. However, contrary to evolved BCDs, the stellar LSB component of I Zw 18 is much more compact than the ionized gas envelope. In the absence of an appreciable underlying stellar population, extended ionized gas emission dominates in the outer parts of I Zw 18, mimicking an exponential stellar disc on optical surface brightness profiles.

Key words. galaxies: dwarf – galaxies: formation – galaxies: evolution – galaxies: structure – galaxies: starburst – galaxies: individual (I Zw 18, II Zw 70, III Zw 102, VII Zw 403, Tol 3, Henize 2-10, IC 4662, Mkn 36, Mkn 71, Mkn 178, Mkn 314, Mkn 324, Mkn 600, NGC 1705, NGC 1800, NGC 5253)

1. Introduction

Since its discovery by Sargent & Searle (1970), I Zw 18 has been looked at as the prototypical blue compact dwarf (BCD) galaxy. Its low oxygen abundance (Searle & Sargent 1972), established in numerous subsequent studies (Lequeux et al. 1979; French 1980; Kinman & Davidson 1981; Pagel et al. 1992; Skillman & Kennicutt 1993; Martin 1996; Vílchez & Iglesias-Parámo 1998; Izotov & Thuan 1998a, 1998b; Izotov et al. 1999) to be 12 + log(O/H) ≈ 7.2 makes it the least chemically evolved star-forming galaxy in the local Universe. Whether this is a signature of youth (cf. e.g. Izotov & Thuan 1998a) remains, however, a subject of debate.

I Zw 18 was described by Zwicky (1966) as a pair of compact galaxies, subsequently shown to be two compact star-forming (SF) regions within the same galaxy with an angular separation of 5.″8, the brighter northwestern (NW) and fainter southeastern (SE) components. Ground-based and *HST* observations have revealed that both regions are embedded in a low-surface brightness (LSB) filamentary envelope extending out to a radius ∼20″ (Davidson et al. 1989; Dufour & Hester 1990; Dufour et al. 1996a; Martin 1996; Östlin et al. 1996), and within an extensive H I halo with a projected size of 60″× 45″ (van Zee et al. 1998b; see also Viallefond et al. 1987).

Send offprint requests to: P. Papaderos,
e-mail: papade@uni-sw.gwdg.de

⋆ Based on observations with the NASA/ESA *Hubble Space Telescope*, obtained at the Space Telescope Science Institute, which is operated by AURA, Inc., under NASA contract No. NAS 5–26555.

⋆⋆ Obtained at the German–Spanish Astronomical Center, Calar Alto, operated by the Max–Planck–Institute for Astronomy, Heidelberg, jointly with the Spanish National Commission for Astronomy.

⋆⋆⋆ Obtained at the Kitt Peak National Observatory, operated by the Association of Universities for Research in Astronomy, Inc., under cooperative agreement with the National Science Foundation.

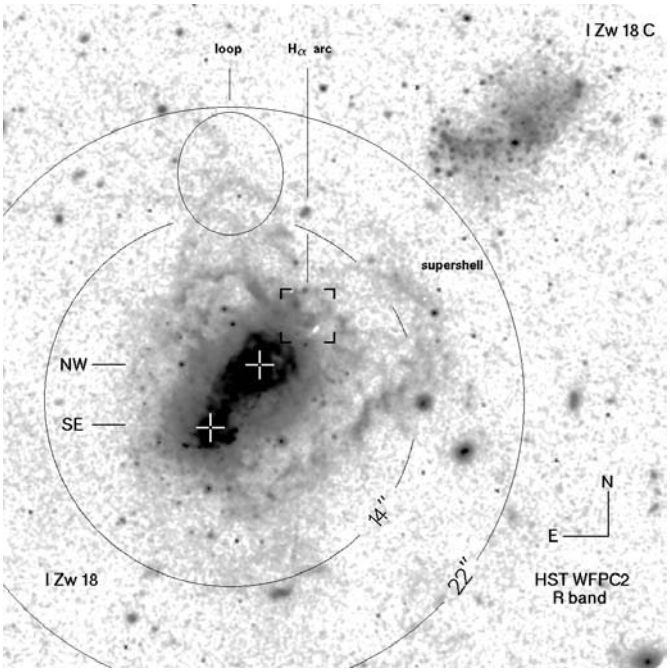

Fig. 1. *HST*/WFPC2 archival image of I Zw 18 in the *R* band. North is at the top and east to the left. The two star forming regions in I Zw 18 are labelled NW and SE. Regions marked *loop* and Hα *arc* have been investigated spectroscopically in Izotov et al. (2001a). The northwestern supershell in I Zw 18 and the detached irregular component I Zw 18 C are indicated. The larger circles with radii 14″ and 22″ are centered between the NW and SE star forming regions.

The spectrophotometric properties of the fainter detached component I Zw 18 C, located ∼22″ northwest of the NW region are still poorly known. Dufour et al. (1996a), Petrosian et al. (1997), Izotov & Thuan (1998a), van Zee et al. (1998b) and Izotov et al. (2001a) have shown it to have the same recession velocity as the main body, thus establishing its physical association to I Zw 18. The SF activity of I Zw 18 C is weak, its Hα equivalent width not exceeding ∼60 Å along the major axis (Izotov et al. 2001a). In spite of deep Keck II spectroscopy, Izotov et al. (2001a) failed to detect oxygen lines, so its oxygen abundance is not known.

Colour-magnitude diagram (CMD) studies, based on *HST* WFPC2 images, suggest for the main body an age between several 10 Myr (Hunter & Thronson 1995; Dufour et al. 1996b) and ∼1 Gyr (Aloisi et al. 1999). Östlin (2000) argues from *HST* NICMOS J and H images that a fit to the J vs. $J-H$ CMD is best achieved with a stellar population with age as high as 5 Gyr. As for I Zw 18 C, Dufour et al. (1996b) and Aloisi et al. (1999) derive an age of a few hundred Myr.

Kunth & Östlin (2000) conclude from optical and NIR surface photometry studies that I Zw 18 possesses an evolved and spatially extended stellar population underlying its SF regions. Their conclusion is based on a nearly constant relatively red $B-R\sim 0.6$ mag and outwards increasing $B-J$ colour of the LSB envelope. Because the latter has a surface-brightness profile that can be well fitted by an exponential law, Kunth & Östlin (2000) ascribed the LSB emission to a stellar disc with an age of ∼5 Gyr.

On the theoretical front, Legrand (2000) and Legrand et al. (2000) in an attempt to explain the paucity of nearby SF dwarf galaxies with oxygen abundance 12 + log(O/H) < 7.2 proposed that these systems form over the Hubble time through a continuous low-level SF process. In this scenario, I Zw 18 would have an extended stellar disc with $m_V\sim 20$ mag and a mean surface brightness ∼28 V mag/□″.

If the presence of a significant old stellar background can be demonstrated then I Zw 18 would be a standard BCD, and the hypothesis of it being a young galaxy must be abandoned. I Zw 18 would then be like the vast majority of BCDs which are evolved dwarf galaxies where star formation is occurring within an extended, circular or elliptical stellar host galaxy (Loose & Thuan 1986, hereafter LT86; Kunth et al. 1988; Papaderos et al. P96a, hereafter P96a). Such systems, classified iE/nE by LT86, account for ∼90% of the local BCD population. Their red LSB underlying component dominates the surface brightness and colour distribution in their outer parts and contributes on average ∼1/2 of their B luminosity within the 25 B mag/□″ isophote (Papaderos et al. 1996b).

The view that I Zw 18 has properties similar to old BCDs, with the exception of its low oxygen abundance, is not well established, however. Stars populating the stellar disc postulated by Legrand et al. (2000) and Kunth & Östlin (2000) have not been seen in I Zw 18 (Izotov & Thuan 2002). By contrast, in CMD studies of Local Group dwarfs (see e.g. Grebel 2001 for a review) and of a few nearby BCDs (cf. Sect. 3.1), a census of several thousands resolved stars unambiguously proves the existence of an evolved and spatially extended stellar background. In fact, the observational evidence for a dominant 1–5 Gyr old stellar population in I Zw 18 rests on a sample of only about one dozen red point sources seen both in the optical and NIR ranges by *HST* (Aloisi et al. 1999; Östlin 2000). Ages quoted from this tiny statistical probe assume no or a uniform extinction, while non-uniform dust absorption in I Zw 18 has been discovered recently (Cannon et al. 2002).

The assumption by Kunth & Östlin (2000) that ionized gas does not dominate the LSB envelope of I Zw 18, thus its colours need not be corrected for gaseous emission before deriving ages, has been disputed by Papaderos et al. (2001) and Izotov et al. (2001a). The latter authors remarked that the mean $B-R$ and $B-J$ colours derived by Kunth & Östlin (2000) and Papaderos et al. (2001) in the outer regions of the main body are entirely consistent with pure ionized gas emission. This is also consistent with the results by Hunt et al. (2002) who placed from deep NIR data an upper limit of $\lesssim$15% to the J band light fraction of stars older than 500 Myr in I Zw 18.

The large range of ages derived previously, together with the unexplored role of extended gaseous emission as well as dust absorption led us to reexamine the photometric structure of I Zw 18. Our goal was to determine whether there exists a stellar LSB component underlying the filamentary envelope of I Zw 18 and extending well beyond the NW and SE regions. If present, how does its colour and structural properties compare to those of standard BCDs, and what implications can be drawn for the evolutionary state of I Zw 18?

The paper is organized as follows. In Sect. 2 we discuss the set of ground-based and *HST* data included in this study

and briefly describe the techniques used in the surface photometry analysis. We consider essential to study the photometric structure of I Zw 18 not in isolation but in the context of the main class of evolved BCDs. The photometric structure of these systems is discussed in Sect. 3 on the example of the nearby iE BCDs Mkn 178 and VII Zw 403. Section 4 focuses on I Zw 18, the distance of which is assumed throughout to be 15 Mpc (Izotov et al. 2001a). In Sect. 4.1 we derive surface brightness profiles (SBPs) of its main body on the usual assumption that its LSB emission is predominantly of stellar origin. The properties of the LSB component after subtraction of nebular line emission (Sect. 4.2) are studied in Sect. 4.3. The photometric structure of I Zw 18 C is discussed in Sect. 4.4. In Sect. 5.1 we compare the structural properties of I Zw 18 with those of standard BCDs. In Sect. 5.2 we investigate whether spatially extended ionized gas emission can mimic the SBP of a red exponential stellar disc. The evolutionary state of I Zw 18 in the light of the present results is discussed in Sect. 5.3. Our conclusions are summarized in Sect. 6.

2. Observations and data reduction

2.1. Data acquisition

Broad-band Johnson B, V and Cousins R, I images of I Zw 18 were taken during three observing runs. A first set of exposures in B (20 min) and R (10 min) was acquired on March 7–10, 1997 with the CAFOS focal reducer attached to the 2.2 m telescope of the German-Spanish Astronomical Center, Calar Alto, Spain. CAFOS was equipped with a 2048 × 2048 SITe CCD operating at a gain of 2.3 e^- ADU^{-1}, with a read-out noise of <3 counts (rms). With a focal ratio of $f/4.4$, the instrumental scale was $0\farcs53$ $pixel^{-1}$ and the usable field of view (FOV) ∼15′. Another series of images, each slightly offset from the others, with a total integration time of 90 min in B and 50 min in R was taken with the Calar Alto 1.23 m telescope in the period January 24 to February 22, 2000. A 2048 × 2048 SITe detector mounted at its Cassegrain focus gave an instrumental scale of $0\farcs5$ $pixel^{-1}$ and a usable FOV of ∼11′. V and I imaging data of I Zw 18 were acquired with the Kitt Peak National Observatory (KPNO) 2.1 m telescope on April 18, 1999. The telescope was equipped with a 1024 × 1024 Tektronix CCD detector operating at a gain of 3 e^- ADU^{-1}, giving an instrumental scale of $0\farcs305$ $pixel^{-1}$ and a FOV of 5′. The total exposure time of 40 and 60 min in V and I, respectively, was split up into four slightly shifted subexposures.

J images were obtained with the 3.5 m telescope at Calar Alto during three consecutive nights (May, 12–14, 2000). The Omega camera, mounted at the prime focus ($f/3.5$) of the telescope, consisted of a 1024 × 1024 pixel Rockwell HAWAII detector yielding a scale of $0\farcs396$ $pixel^{-1}$. The large FOV ($6\farcm76$) as compared to the size of I Zw 18 allowed for dithering ON source. The total on object integration time was 66 min. The data were calibrated by observing UKIRT NIR standard stars from Hunt et al. (1998). The photometric accuracy is estimated to be better than 0.1 mag. A detailed presentation of the data acquisition and reduction will be given in Noeske et al. (2002).

Table 1. Summary of the observational data.

Object	Year	Telescope	Observations (min)
I Zw 18	1997	Calar Alto/2.2 m	B(20), R(10)
	1999	KPNO/2.1 m	V(40), I(60)
	2000	Calar Alto/3.5 m	J(66)
	1994	*HST*/WFPC2	B(77), V(77), R(90)
			Hα(77), [O III](77)
Mkn 178	1997	Calar Alto/2.2 m	B(17), R(12)
	2000	Calar Alto/1.23 m	B(53), R(63)
VII Zw 403	1994	Calar Alto/2.2 m	B(60), R(20)
	1997	Calar Alto/2.2 m	B(20), R(10), Hα(25)
	1995	*HST*/WFPC2	V(70), I(70), Hα(40)

Data on the iE BCDs Mkn 178 and VII Zw 403 (Sect. 3.1) are based on Johnson B and Cousins R images taken at Calar Alto during three observing runs. VII Zw 403 was observed with the 2.2 m Calar Alto telescope in February 1994 for 60 min in B and 20 min in R. Additional B (20 min), R (10 min) and Hα (25 min) images for this galaxy were taken with the 2.2 m/CAFOS during the 1997 run (see above). During the same run Mkn 178 was observed in B and R for 17 min and 12 min, respectively. A third set of broad-band images of Mkn 178 with a total exposure of 53 min in B and 63 min in R was taken with the Calar Alto 1.23 m telescope in the period January–February, 2000.

The $FWHM$ of point sources in all observing runs was in the range between $1\farcs05$ and $1\farcs6$. Bias and flat–field frames were obtained during each night of the observations. Calibration was accomplished by observing standard fields from Landolt (1992) and Christian et al. (1985). Our calibration uncertainties are estimated to be below 0.05 mag in all bands. Standard reduction steps, including bias and flat–field correction, cosmic ray rejection and image co-alignment were carried out using the ESO MIDAS[1] and IRAF[2] software packages.

We have also included in the present study archival *HST*/WFPC2 B (F450W), V (F555W) and R (F702W) images of I Zw 18 (PI: Dufour, GO-5434, November 1994). These have the advantage of including both the main body and the C component in their FOV (cf. Dufour et al. 1996b). In order to estimate the luminosity contribution of ionized gas emission (Sect. 4.2) we use narrow-band [O III] λ5007 (F502N) and Hα (F658N) archival *HST*/WFPC2 images. In the photometric study of VII Zw 403 we use archival *HST*/WFPC2 V, I and Hα images (PI: Westphal, GO-6276, July 1995). These data have been discussed in detail by Lynds et al. (1998), Schulte-Ladbeck et al. (1998, 1999a) and Izotov & Thuan (2002). The *HST* photometry was transformed to the standard Johnson-Cousins $UBVRI$ photometric system following the prescriptions of Holtzman et al. (1995). The observational data discussed in Sects. 3 and 4 are summarized in Table 1.

[1] Munich Image Data Analysis System, provided by the European Southern Observatory (ESO).

[2] IRAF is the Image Reduction and Analysis Facility distributed by the National Optical Astronomy Observatory, which is operated by the Association of Universities for Research in Astronomy (AURA) under cooperative agreement with the National Science Foundation (NSF).

2.2. Surface photometry

In the surface photometry analysis of the iE BCDs Mkn 178 and VII Zw 403 (Sect. 3.1) we use improved versions of the techniques described in P96a. For intermediate and low surface brightness levels, the equivalent radius $R^* = \sqrt{A(\mu)/\pi}$ corresponding to the surface brightness μ was computed by a combination of methods i) (the area $A(\mu)$ is determined by fitting an ellipse to the isophote) or ii) (a line integral is calculated along the respective isophote in polar and cartesian coordinates). In the high-surface-brightness (HSB) regime, where several star forming regions can be distinguished on ground-based images, $A(\mu)$ was computed using method iii) (summation of all pixels inside a polygonal aperture with a surface brightness $\leq \mu$).

By definition, these methods trace the growth of the angular size of a galaxy with increasing μ, so that the equivalent radius R^* is a monotonic function of surface brightness. Because no subjective assumptions are made on the geometrical center or the mean position angle and ellipticity at any intensity interval, they allow to derive the surface brightness distribution in a "standard" and reproducible manner for BCDs that are morphologically very different.

While these techniques work well for most BCDs, they should be used with caution in the rare case of an extremely irregular and patchy LSB morphology, where either ellipses give a poor geometrical approach to isophotes or the LSB envelope consists of several detached entities.

One such example is the main body of I Zw 18 which shows an irregular morphology in the LSB outer regions. As verified from ground-based and *HST* data, the SBP slope derived for $\mu \gtrsim 24$ B mag/$\Box''$ using method i), changes depending on whether some compact and diffuse feature in the periphery of the BCD is included or not (e.g. features along the northwestern supershell, cf. Fig. 1). Method ii) which is best suited when $A(\mu)$ is given by a single well-defined isophote, fails when applied to the patchy morphology of I Zw 18. As for method iii), its applicability is restricted to an intensity level typically higher than $\sim 3 \times$ sky noise even for adaptively smoothed images.

We therefore supplemented methods i) through iii) with another flux-conserving technique which allows for a reasonable compromise between the following requirements: a) R^* is a nearly monotonic function of μ, a criterion which guarantees compatibility with methods i)–iii), b) no implicit assumption is made on the morphology of a BCD at any surface brightness level and c) the colour obtained for a given R^* via SBP subtraction is assigned to one and the same region of a BCD in all images. This ensures that the colour profile in the central part is not affected when the brightest SF region does not coincide with the bluest one (see discussion in P96a).

This method (referred to in the following as iv) allows to account optimally for the morphology of a BCD at all intensity levels. The input to method iv) is a set of coaligned multiwavelength frames with the same instrumental scale and point spread function (PSF), previously cleaned for bright foreground and background sources. A reference frame $\mathcal{F}$ is first computed from the signal-to-noise weighted average of the input images. This step incorporates an adaptive resolution pattern that allows to conserve small-scale intensity enhancements in the SF region while approaching a chosen resolution of typically $\lesssim 3 \times$ PSF in the LSB regime. $\mathcal{F}$ serves as a template for computing a series of masks ($n_{\rm mask}$) mapping equidistant logarithmic intensity intervals between $I_{\rm min}$ and $I_{\rm max}$. A pixel in the mask m_i ($i \leq n_{\rm mask}$) is set to unity when its intensity F is such that $I - \Delta I \leq F \leq I$ and to zero otherwise. Each input frame is then in turn weighted by the mask m_i and used to compute the mean surface brightness within the mask area set to unity.

The radius $R^*(\mu)$ corresponding to the mask m_i is given by

$$R^*(\mu) = \sqrt{\left(\frac{A_I + A_{I-\Delta I}}{2\pi}\right)}, \quad (1)$$

where A_I and $A_{I-\Delta I}$ denote respectively the areas of frame $\mathcal{F}$ in $\Box''$ with intensity levels above I and $I - \Delta I$.

A virtue of method iv) as compared to iii), is that the surface brightness μ is not a user-defined input variable, but is computed from *all* pixels within a galaxy's region of arbitrary shape. This allows to overcome the problem of the artificial SBP flattening at low intensities inherent to method iii) (see discussion in P96a and Cairós et al. 2001a). On the other hand, method iv) requires an accurate subtraction of bright foreground and background sources, especially in the LSB regime. This is because, in the presence of a faint ($\mu_B \gtrsim 25$ mag/$\Box''$) LSB background, a moderately bright source may affect the photon statistics and colours computed within the mask m_i. Tests on the iE BCDs Mkn 178 and VII Zw 403 (Sect. 3.1) as well as on other SF dwarfs with a variety of morphologies (cf. Noeske et al. 2002) have shown that method iv) is reliable down to a faint intensity level and gives indistinguishable results from methods i)–iii) for the *plateau* (see Sect. 3.1) and the LSB components. Methods iv) and iii) were used to derive the surface brightness distribution of the main body of I Zw 18 (Sect. 4) in its LSB and HSB regimes.

3. The photometric structure of standard BCDs

This section contains a brief overview of the photometric properties of iE BCDs, the most common type of BCDs (LT86), for later comparison with I Zw 18 (Sect. 5). Surface photometry studies of individual BCDs can be found in e.g. P96a, Vennik et al. (1996, 2000), Doublier et al. (1997, 1999), Marlowe et al. (1997, 1999), Telles et al. (1997), Chitre & Joshi (1999), Makarova (1999), Smoker et al. (1999) and Cairós et al. (2001a).

We focus here on two nearby iE systems, VII Zw 403 and Mkn 178. They were selected for the following reasons: (a) As indicated by surface photometry (Sect. 3.1) and CMD studies, both are bona fide old BCDs. Furthermore, their distances have been accurately determined from the tip of the red giant branch stars to be 4.4 Mpc for VII Zw 403 (Lynds et al. 1998; Schulte-Ladbeck et al. 1999b) and 4.2 ± 0.5 Mpc for Mkn 178 (Schulte-Ladbeck et al. 2000). (b) Neither galaxy shows signatures of a strong past or ongoing interaction (Noeske et al. 2001, 2002), i.e. they are suitable for studying non-tidally triggered SF in BCDs. (c) The central surface brightnesses and exponential scale lengths of their LSB underlying components are intermediate between the main class of BCDs and dwarf irregulars

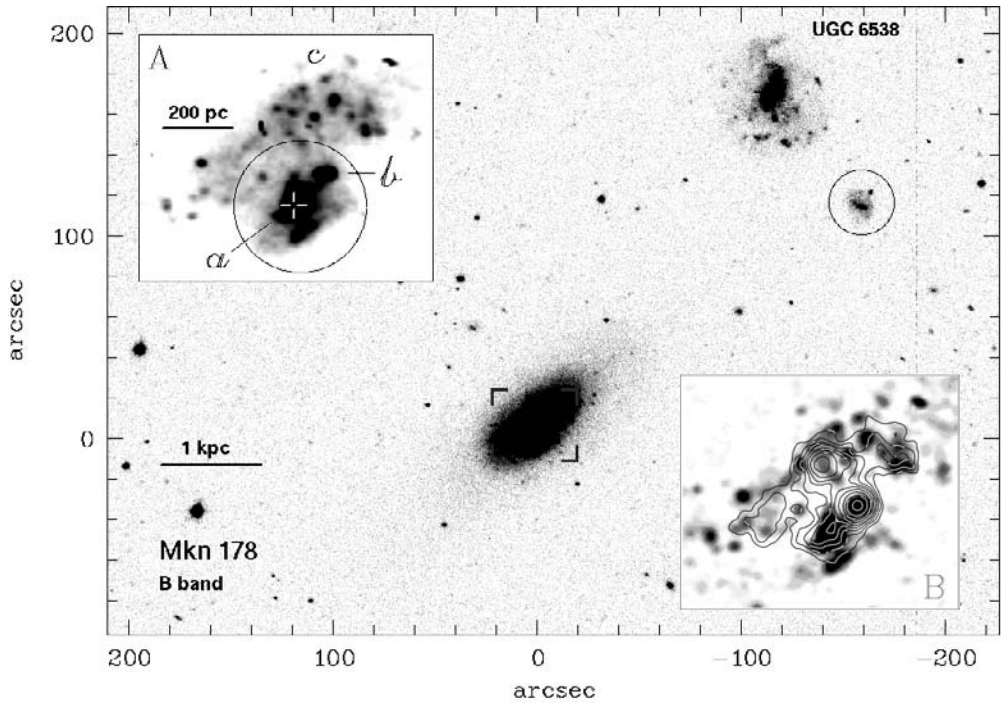

Fig. 2. *B* image of the iE BCD Mkn 178 (D = 4.2 Mpc, Schulte-Ladbeck et al. 2000). The background galaxy UGC 6538 (z = 0.0106) is indicated. The redshift of the encircled galaxy is not known. Insets A and B display magnified versions of the central 41.″5 × 35″ region of Mkn 178. The encircled region in inset A (diameter = 19″) corresponds approximately to the field photographed with *HST*/NICMOS by Schulte-Ladbeck et al. (2000). The star-forming region *a* together with the redder adjacent knot *b* and the extended northern region *c* (notation adopted from González-Riestra et al. 1988) are indicated. Inset B shows NIR contours in the *H* band overlayed on a contrast-enhanced version of A. The *H* emission displays two maxima, the main one coinciding with knot *b* and the secondary one located 8.″4 to the northeast (Noeske et al. 2002).

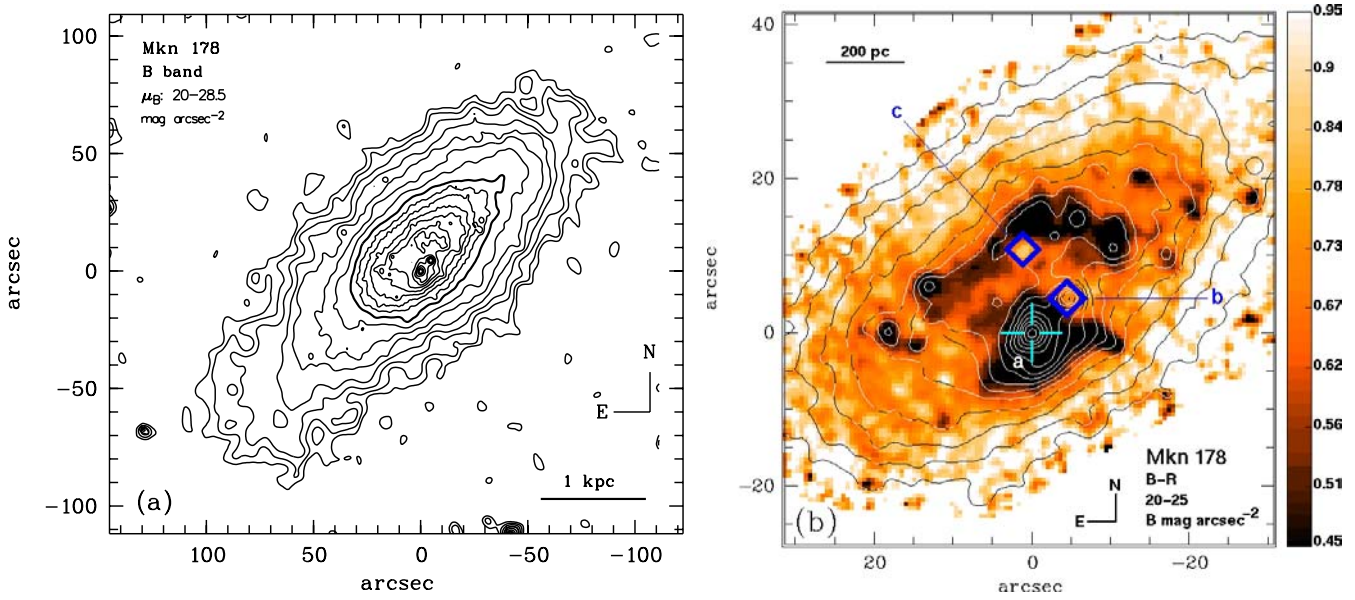

Fig. 3. a) *B* contour map of Mkn 178. Contours correspond to surface brightness levels from 20 to 28.5 mag/□″ in steps of 0.5 mag. The 25 *B* mag/□″ isophote is shown as a thick contour. Note the slight southeastern elongation of the LSB component for $\mu \gtrsim 27$ *B* mag/□″. **b)** $B - R$ map of the central region of Mkn 178 in the range 0.45–0.95 mag, overlayed with *B* contours from 20 to 25 mag/□″. The bluest region ($B - R \approx 0.1$ mag) is associated with the brightest region *a* while the optically fainter region *b* coincides with the brightest of the *H* sources (depicted by rhombs) detected by Noeske et al. (2002, cf. inset B in Fig. 2). Beyond the outermost contour (25 *B* mag/□″), the colour is dominated by the red ($B - R \sim 1.1$ mag) stellar LSB component underlying the star-forming regions.

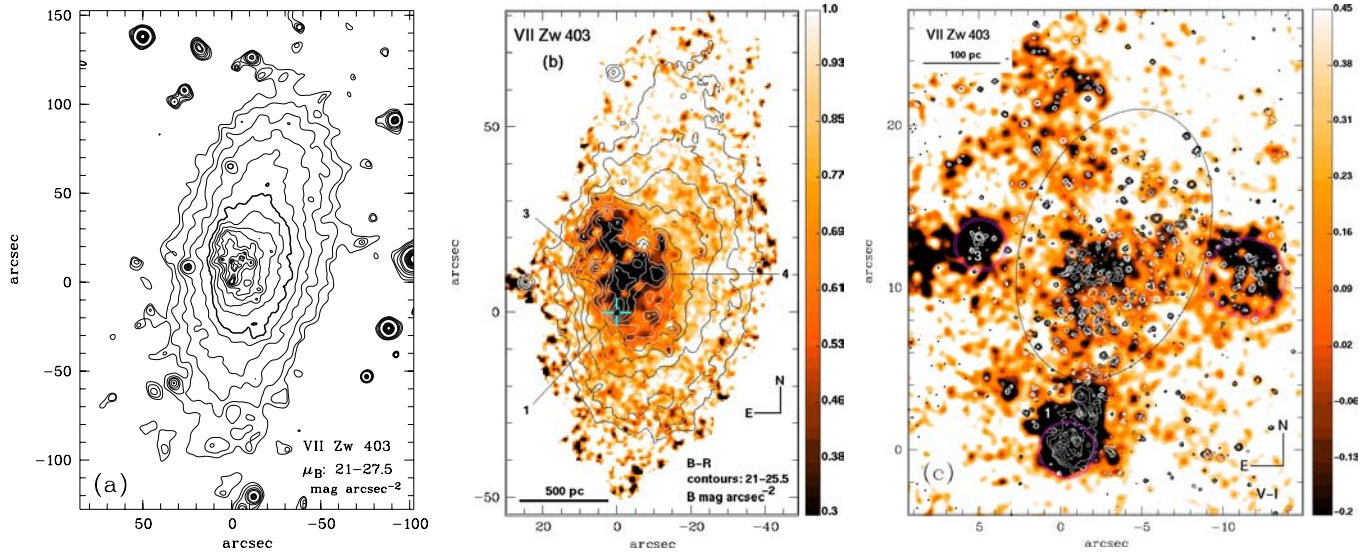

Fig. 4. a) Contour map of VII Zw 403 with surface brightness levels from 21 to 27.5 B mag/□″ in steps of 0.5 mag. The 25 B mag/□″ isophote is shown by the thick contour. **b)** $B-R$ map of VII Zw 403 in the range 0.3–1.0 mag, overlayed with B contours. The position of the bright stellar assemblies 1 (cross at axes' origin), 3 and 4 (notation adopted from Fig. 2 of Lynds et al. 1998) is indicated. Note the blue (∼0.2 mag) featureless region protruding between regions 3 and 4, up to ∼30″ to the northeast of region 1. **c)** $V-I$ map of the central portion of VII Zw 403 computed from archival *HST*/WFPC2 data. Contours, derived from a contrast-enhanced V image, delineate the spatial distribution of compact sources in the high-surface-brightness regime of the BCD. Comparison with Fig. 6 shows that the blue ($V-I \leq -0.2$) regions in the periphery of bright young stellar assemblies are spatially correlated with the bright Hα features, suggesting that ionized gas emission produces significant colour changes on scales of a few tens of pc.

(dIs). Therefore the discussion below is not concerned with extreme ultra-compact BCDs, which may undergo intermittent very violent SF episodes, but rather with average BCDs/dIs where star formation *may* proceed at a lower rate over longer periods.

3.1. Mkn 178 and VII Zw 403

The SBP of Mkn 178 (Fig. 5a) reveals three main intensity regimes, as is commonly seen in iE BCDs. At small radii ($R^* \leq 150$ pc), it exhibits a narrow excess due to the luminosity contribution of regions a and b (cf. inset A in Fig. 2). Region a ($M_B = -12$ mag), contributes ∼40% of the B light in excess to the LSB component. The large colour contrast between this bright assembly of SF sources and its surroundings is reflected on the inner part of the colour profile (Fig. 5b), which rises steeply within $R^* \lesssim 0.2$ kpc from 0.1 mag to ∼0.6 mag. The fainter ($M_B \approx -10.6$ mag) source b ($B-R =$ 0.67 mag) is barely seen on the colour map (Fig. 3b). This is in agreement with the results by González-Riestra et al. (1988) who found also a colour difference between regions a and b (cf. their Figs. 3a–c) and established spectroscopically that region b is part of Mkn 178. Interestingly, NIR imaging by Noeske et al. (2002) shows the optically faint source b to be coinciding with the surface brightness maximum in the H band (inset B in Fig. 2), whereas region a is nearly absent on NIR images.

The second intensity regime, with surface brightnesses between ∼22 and ∼25 B mag/□″, represents the total luminosity of compact and diffuse sources in the inner ∼0.65 kpc of Mkn 178 (Fig. 2). This pronounced bump, referred to as *plateau* in P96a[3], is a common feature in SBPs of iE BCDs. Its intensity distribution has been approximated in the decomposition scheme of P96a by a Sérsic profile (Sérsic 1968) with exponent η in the range $1 \lesssim \eta \lesssim 5$. The isophotal radius P_{25} of the plateau at the surface brightness level of 25 mag/□″ (cf. panels a and c of Fig. 5) measures the radial extent of the SF component in BCDs (P96a). The plateau radius of ∼450 pc of Mkn 178 (Fig. 5a) together with the moderately red $B-R =$ 0.6–0.8 mag at HSB levels (Fig. 3b) suggests a mild SF activity on a spatial scale of ∼1 kpc.

Signatures of a spatially extended, young stellar population are also present on the $B-R$ map of VII Zw 403 (Fig. 4b), revealing blue colours inside its 24 B mag/□″ isophote. The case of VII Zw 403 illustrates the situation where, depending on the optical colour considered, the brightest region within the plateau may not coincide with the bluest one. The $B-R$ colour of the three bright SF regions indicated in Fig. 4b (0.33–0.55 mag) is on average redder than that of the diffuse stellar population surrounding them (0.12–0.23 mag). The opposite trend is observed on the $V-I$ map (Fig. 4c), where the surroundings of bright stellar clusters are bluer (–0.18–−0.38 mag) than the smoothly distributed stellar population within the ellipse ($V-I = 0.1$–0.3 mag). Comparison of Figs. 4c and 6 reveals that the regions with blue $V-I$ are

[3] The same feature has been called *platform* by Telles et al. (1997) or *core* by Marlowe et al. (1999, see their Fig. 1). SBPs of BCDs that cannot be approximated by a simple fitting law (e.g. a de Vaucouleurs or exponential distribution) because of a pronounced *plateau* feature at intermediate intensity levels, have been classified as *dd (double)* by Telles et al. (1997) or *composite* by Doublier et al. (1999) and Cairós et al. (2001a).

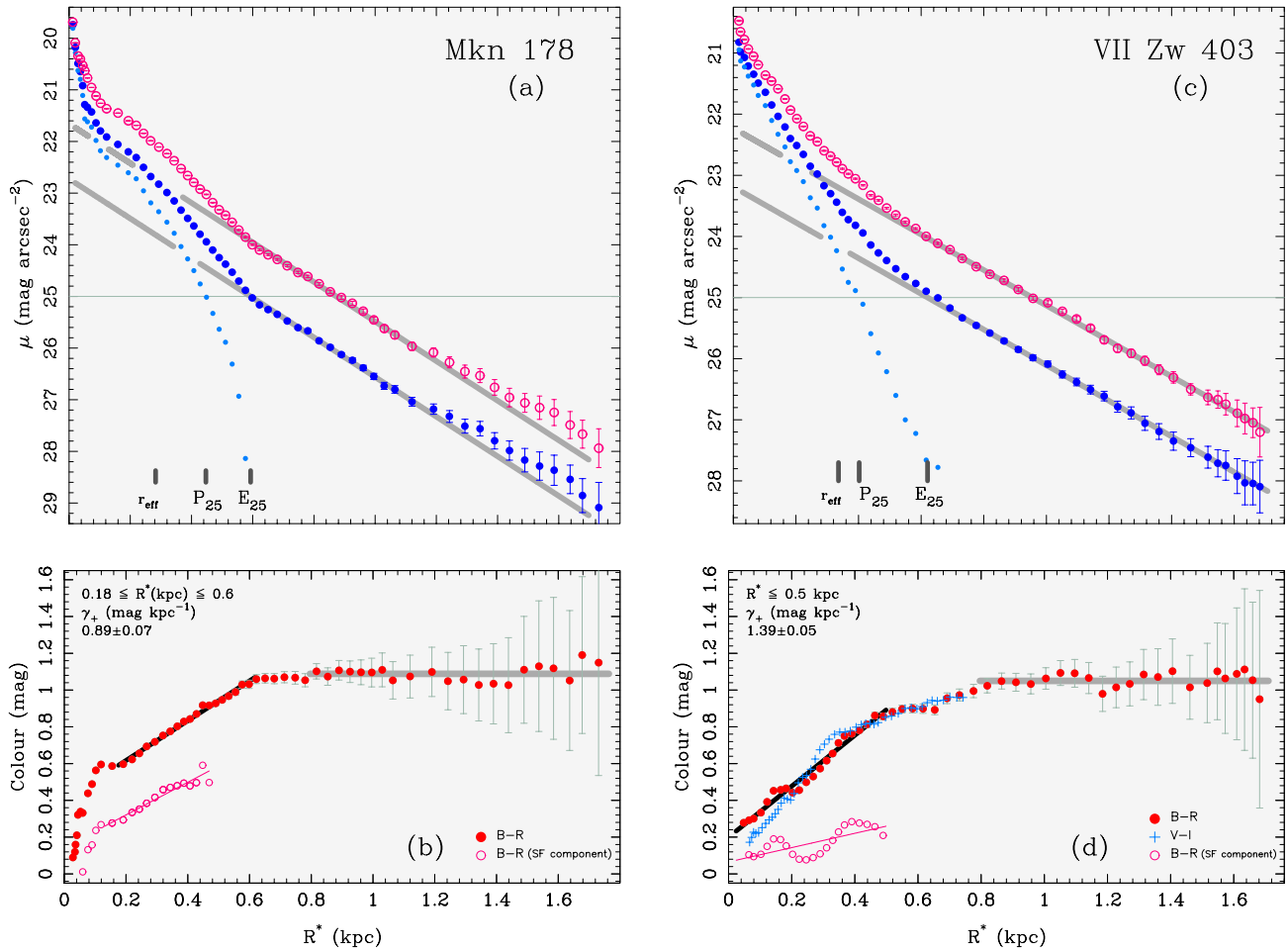

Fig. 5. a) Extinction-corrected B (filled circles) and R (open circles) surface brightness profiles (SBPs) of Mkn 178 vs. equivalent radius R^*. Thick-gray lines show exponential fits to the LSB component in the range $0.6 \leq R^*$ (kpc) ≤ 1.2. The slight flattening with respect to the exponential fit for $R^* > 1.2$ kpc is caused by the southeastern extension of the BCD (Fig. 3a), which accounts for $\lesssim$2% of the LSB light in B. The intensity profile which is represented by small filled circles is obtained by subtracting the exponential fit from the B band SBP. This excess emission is due to the young and intermediate-age stellar populations within the plateau component. It contributes ~60% of the B light of Mkn 178 inside its 25 B mag/□″ isophote. The isophotal radius of the plateau (P_{25}), that of the LSB component (E_{25}) and the effective radius $r_{\rm eff}$ in B are indicated. The line-of-sight contribution of the plateau population to the B intensity decreases from <40% at P_{25} to $\lesssim$4% at E_{25}. **b)** $B-R$ profile of Mkn 178. For 0.2 kpc $\lesssim R^* \lesssim E_{25}$ the $B-R$ increases linearly with a gradient $\gamma_+ \approx 0.9$ mag kpc^{-1}. For $R^* > E_{25}$ the colour becomes constant at $B-R \approx 1.1$ mag and is due to the red stellar LSB population. The solid grey line results from the subtraction of the fits to the B and R SBPs of the LSB component. Open circles show the colour distribution within P_{25} after correction for the luminosity contribution of the LSB host (see discussion in the text). While this correction has no effect on γ_+, it shifts the $B-R$ profile by ≈–0.4 mag. **c)** and **d)** Surface brightness and colour profiles of VII Zw 403. Symbols have the same meaning as in panels **a)** and **b)**. Panel **d)** also shows the $V-I$ profile derived from archival *HST*/WFPC2 data. Correction for the emission of the LSB component results in a downwards shift of the $B-R$ colour profile and a decrease in γ_+ from ~1.4 mag kpc^{-1} to ~0.4 mag kpc^{-1}.

spatially correlated with the Hα emission and are more extended than the ionizing stellar sources. The combination of blue $V-I$ (<0 mag) with red $B-R$ (~0.4–0.6 mag) colours is a sign of intense nebular emission on scales of a few tens of parsecs around SF regions in VII Zw 403 (cf. e.g. Izotov et al. 1997; Papaderos et al. 1998; Noeske et al. 2000; Guseva et al. 2001).

The plateau component of Mkn 178 ($0.2 \lesssim R^*$ (kpc) $\lesssim 0.65$) shows a roughly linear colour increase with a gradient γ_+ of ≈0.9 mag kpc^{-1} (Fig. 5b). This is also the case for VII Zw 403 (Fig. 5d) where $\gamma_+ \approx 1.4$ mag kpc^{-1}, in the upper range of values for iE/nE BCDs (0.2–1.6 mag kpc^{-1}) in the P96a sample. A large $V-I$ gradient (1.67 ± 0.1 mag kpc^{-1}) is also obtained from archival *HST*/WFPC2 data in the radius range $0.1 \lesssim R^*$ (kpc) $\lesssim 0.5$.

The gradual colour increase inside the plateau comes along with a population gradient in VII Zw 403. CMD studies by Schulte-Ladbeck et al. (1999b) reveal that the surface density of red stars in this BCD decreases slower with radius than other types of stars, implying that they dominate in the outer parts of VII Zw 403. Such a spatial segregation with young blue stars in the inner part ($R^* \lesssim P_{25}$) of BCDs, and old red stars in the outer regions has also been reported in CMD studies of Mkn 209 (Schulte-Ladbeck et al. 2000), NGC 1569 (Aloisi et al. 2001), UGCA 290 (Crone et al. 2002) and NGC 1705 (Tosi et al. 2001).

Table 2. Structural properties of the iE BCDs Mkn 178 and VII Zw 403[a].

Name	Band	$\mu_{E,0}$	α	$m^{\rm fit}_{\rm LSB}$	P_{25}	$m_{P_{25}}$	E_{25}	$m_{E_{25}}$	$m_{\rm SBP}$	$m_{\rm tot}$	$r_{\rm eff}$,r_{80}
		mag/□″	pc	mag	pc	mag	pc	mag	mag	mag	pc
(1)	(2)	(3)	(4)	(5)	(6)	(7)	(8)	(9)	(10)	(11)	(12)
Mkn 178	*B*	22.72 ± 0.04	283 ± 4	15.01	447	15.00	593	15.53	14.25 ± 0.02	14.25	283,569
	R	21.66 ± 0.03	284 ± 4	13.94	479	14.78	873	14.17	13.52 ± 0.02	13.51	350,704
VII Zw 403	*B*	23.19 ± 0.07	372 ± 10	14.99	402	15.50	620	15.75	14.47 ± 0.02	14.46	336,776
	R	22.23 ± 0.20	374 ± 18	14.01	422	15.34	955	14.36	13.77 ± 0.02	13.76	440,896

[a] Distances of 4.2 Mpc and 4.4 Mpc have been adopted for Mkn 178 and VII Zw 403, respectively (Schulte-Ladbeck et al. 1999b; Schulte-Ladbeck et al. 2000). The tabulated values are corrected for Galactic extinction (A_B = 0.078 mag for Mkn 178 and 0.09 mag for VII Zw 403).

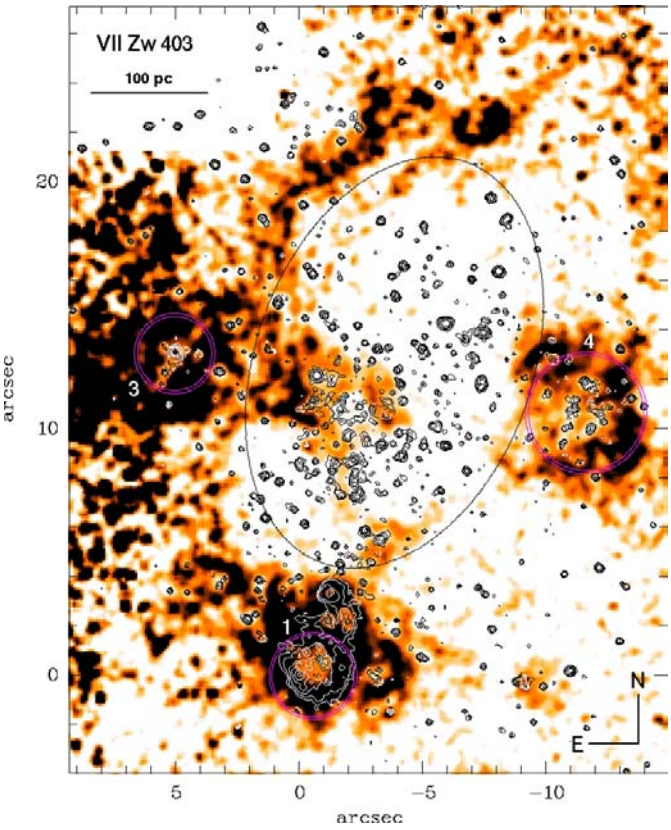

Fig. 6. Hα map of VII Zw 403 from archival *HST*/WFPC2 images. Three of the bright stellar assemblies studied by Lynds et al. (1998) are indicated by circles. Contours show the spatial distribution of bright stellar sources in *V* (cf. Fig. 4c).

We turn next to the exponential LSB component which dominates the light for $\mu \gtrsim 25$ *B* mag/□″. The evolved state of the host galaxy of Mkn 178 is evident from its red $B-R$ colour which levels off at 1.08 ± 0.04 mag for $R^* \gtrsim E_{25}$ (cf. Fig. 5b). The red optical colour, together with $J-H = 0.53 \pm 0.13$ mag and $H-K = 0.25 \pm 0.12$ mag (Noeske et al. 2002) for the LSB component support the conclusion by Schulte-Ladbeck et al. (1998) that Mkn 178 is not young. This is also the case for the LSB host of VII Zw 403 for which we derive a mean $B-R$ colour of 1.05 ± 0.04 mag, in good agreement with the value of ≈1.12 mag of Schulte-Ladbeck & Hopp (1998), after correction for extinction (A_B = 0.09 mag). The $B-R$ colour is also consistent with $V-I = 0.92 \pm 0.05$ mag obtained from *HST*/WFPC2 data at $R^* = 0.75$ kpc (cf. Fig. 5d).

A substantial colour gradient, as typical property of BCDs inside a galactocentric distance slightly larger than P_{25} (P96a) may reflect both, a true stellar age gradient and an outwards decreasing line-of-sight contribution of a young stellar population relative to the red underlying LSB host. By contrast, the majority of dIs exhibit no or minor colour gradients. van Zee (2001) reports strong colour gradients (up to $\gamma_+(B-V) = 0.5$ mag kpc^{-1}) only for those dIs with significant ongoing SF. Interestingly, these are compact systems, the scale length of their LSB host being comparable to those of BCDs (≲0.5 kpc). However, the majority of dIs are quiescent and have small colour gradients, not exceeding $\gamma_+(B-V) = 0.2$ mag kpc^{-1} (Patterson & Thuan 1996; van Zee 2001).

The effect of the light of the evolved stellar LSB host on the luminosity-weighted BCD colour within P_{25} is illustrated in Figs. 5b and 5d. We show with open symbols the $B-R$ profile as computed from the light in excess to the exponential fit, i.e. with the LSB emission subtracted out. For Mkn 178 this correction has virtually no effect on γ_+, it shifts, however, the colour profile by about –0.4 mag. The situation is different for VII Zw 403, where subtraction of the contribution of the LSB component changes the colour gradient from $\gamma_+ \sim 1.4$ mag kpc^{-1} to ∼0.4 mag kpc^{-1}. These corrections depend sensitively on the model adopted for the intensity distribution of the LSB host and, in particular on whether or not the exponential slope in the outer parts is extrapolated all the way to $R^* = 0$ (see discussion in e.g. P96a and Cairós et al. 2002). They cannot be neglected, however, in the majority of BCDs, as the central surface brightness of their red LSB host is typically brighter than 22 *B* mag/□″ (cf. Fig. 13).

In Table 2 we summarize the derived photometric properties of Mkn 178 and VII Zw 403. Columns 3 and 4 list respectively the central surface brightness $\mu_{\rm E,0}$ and scale length α of the LSB host as obtained from exponential fits to the outer part of SBPs, and weighted by the photometric uncertainty of each point. The corresponding total magnitude $m^{\rm fit}_{\rm LSB} \approx \mu_{\rm E,0} - 5\log(\alpha'') - 2$ of the LSB host for a pure exponential distribution is given in Col. 5. Columns 6 through 9 list quantities obtained from profile decomposition. Columns 6 and 8

give respectively the isophotal radii P_{25} and E_{25} of the SF and LSB components, both determined at 25 mag/□″. The respective apparent magnitudes of each component within P_{25} and E_{25} are listed in Cols. 7 and 9. Total magnitudes of the BCD obtained from SBP integration out to the last point, and from flux integration within a polygonal aperture are listed respectively in Cols. 10 and 11. Note that the magnitudes in Cols. 10 and 11 have been derived after removal of compact moderately bright sources in the LSB component. Column 12 gives the effective radius $r_{\rm eff}$ and the radius r_{80} which encircles 80% of the galaxy's total flux.

3.2. The star-forming component in BCDs

In addition to the ongoing SF in several stellar clusters, Mkn 178 and VII Zw 403 contain also in the inner part of their LSB host a more diffuse relatively blue stellar population contributing to the light of the plateau in optical SBPs. Taking into account the effects of nebular line emission, patchy dust absorption and the red underlying LSB background on broad-band colours, both surface photometry and CMD studies suggest that the stellar population responsible for the plateau in Mkn 178 and VII Zw 403 cannot have formed in a single burst. Synchronization of SF over a spatial scale of ∼1 kpc (∼2 P_{25}) requires a time scale of ∼50 Myr, assuming a sound speed velocity in the warm interstellar medium (ISM) of the order of 10 km s^{-1}. CMD studies of Mkn 178 (Schulte-Ladbeck et al. 2000) and VII Zw 403 (Schulte-Ladbeck et al. 1999b) also suggest that both systems experienced extended (several 10^8 yr) periods of star formation, in agreement with theoretical predictions of the evolution of gas-rich dwarfs (e.g. Rieschick & Hensler 1999; Noguchi 2001). This is in contrast to the "standard" picture of star formation in BCDs, of short (∼5 Myr) bursts separated by long (∼1 Gyr) quiescent phases (see e.g. Thuan 1991).

On the other hand, it is not yet clear whether the extended star formation scenario can be generalized to all BCDs. So far, no consensus has been reached concerning the intrinsic or environmental properties which control star formation in these systems (see e.g. Papaderos et al. 1996b; Marlowe et al. 1999; Meurer et al. 1998; Vílchez 1995; Popescu et al. 1999; Pustilnik et al. 2001; Noeske et al. 2001). Evolutionary synthesis models still lend support to the hypothesis of short episodic bursts (Mas-Hesse & Kunth 1999) with an amplitude being possibly inversely related to the mass of the BCD (Krüger et al. 1995). Also, Papaderos & Fricke (1999) have suggested that the burst duration in BCDs is anticorrelated with the central mass density ρ_* of their underlying LSB component. ρ_* was found in the BCD sample of P96a to increase with decreasing mass, being typically by a factor ∼10 larger than in dIs. It is thus conceivable that the large range covered by BCDs with respect to ρ_* may result in a wide diversity in their SF histories.

The structural properties of the LSB component may also influence the spatial extent of SF regions in BCDs. Papaderos et al. (1996b) have remarked that the plateau radius P_{25} is typically ∼1/2 of the isophotal radius E_{25} of the LSB component. They also reported a trend for the fractional area of the SF component of BCDs to increase with decreasing mass of the stellar LSB host. The structural properties of the stellar LSB component appear to influence the global star formation process in dIs also. Hunter et al. (1998; see also Youngblood & Hunter 1999; Heller et al. 2000) have found that the azimuthally averaged star formation rate (SFR) per unit area in dIs scales with the surface density of their stellar LSB component, with the H II regions being typically confined within E_{25} (Roye & Hunter 2000). Perhaps a key result reported recently for dIs is a trend between the average SFR per unit area and the central surface brightness of the stellar LSB population (van Zee 2001).

These empirical lines of evidence suggest that the temporal and spatial occurrence of SF activity in gas-rich dwarfs is not entirely dictated by their Dark Matter halo (cf. e.g. Meurer et al. 1998) but is significantly influenced by the gravitational potential of their evolved host galaxy as well. In view of the age discussion for I Zw 18 (Sect. 5.3), it is important to bear in mind that SF does not occur uniformly over the whole optical extent of a typical BCD, but is generally confined to $R^* < E_{25}$, as shown by both surface photometry and CMD studies. The confinement of SF activity to the central part of BCDs and compact dIs manifests itself in an appreciable colour contrast between the SF component and the LSB periphery (Sect. 3.2).

4. The photometric structure of I Zw 18

4.1. Surface photometry of the main body

In this section we derive SBPs of the main body of I Zw 18 without correction for ionized gas emission. For iE/nE BCDs, this is generally well justified for $R^* > r_{\rm eff}$, as equivalent widths (*EW*) of the nebular emission lines, when averaged over the SF component, are typically smaller than the width of the broad-band filters (e.g., $EW(\mathrm{H}\alpha) < 500$ Å; Salzer et al. 1989; Terlevich et al. 1991; Thuan et al. 1995; Izotov & Thuan 1998b; Guseva et al. 2000; Hopp et al. 2000).

Since we wish to study the unresolved LSB emission in I Zw 18, we first replaced compact sources in its periphery ($R^* \gtrsim 8''$ for ground-based images) by the mean intensity level of adjacent regions (cf. Sect. 2.2). No attempt has been made to screen out filamentary features in the LSB envelope of I Zw 18. Since the identification of diffuse Hα shells depends on the resolution and depth of a given data set, doing so could affect colours derived from intercomparison of ground-based and *HST* SBPs. We have evaluated the effect of this correction on the profile slope by masking out extended filamentary features (such as the northwestern supershell; Fig. 1). We have also compared SBPs derived prior to the subtraction of bright compact sources and after adding faint ($m_B \geq 22$ mag) artificial stars at various locations in the LSB envelope. Depending on the method used (Sect. 2.2), a selective rejection of compact and diffuse features may result in a variation of up to 30% in the SBP slope at low intensity levels.

Figure 7a shows that the ground-based *B*, *V*, *R* and *J* SBPs of I Zw 18 can be well fitted by an exponential law in the radius range $8'' \leq R^* \lesssim 16''$ (thick line). This gives for the LSB envelope a central surface brightness $\mu_{\rm E,0} = 22.3 \pm 0.1$ *B* mag/□″ and an exponential scale length $\alpha \sim 250$ pc (Table 3). From

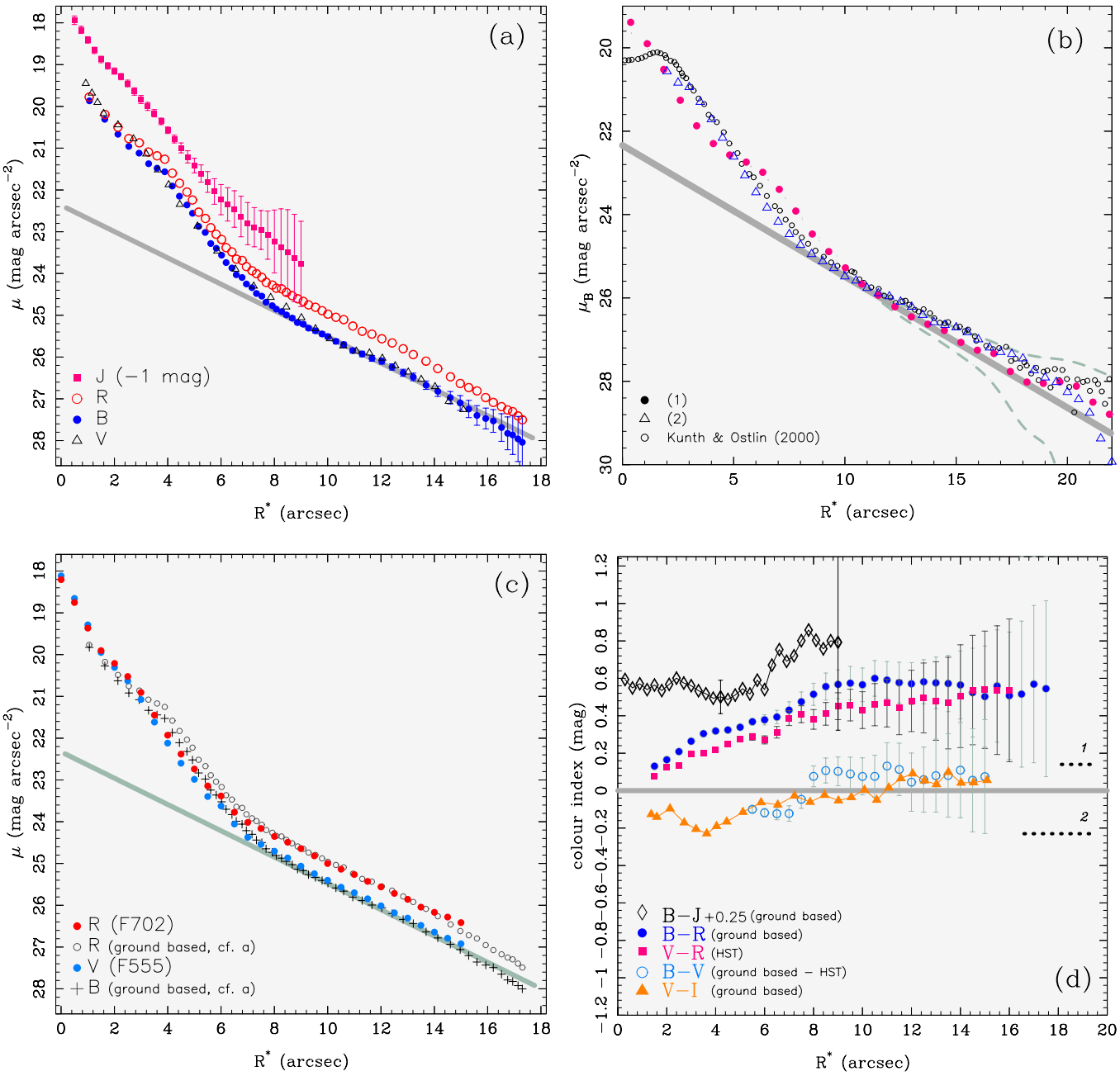

Fig. 7. a) B, V, R and J SBPs of I Zw 18 as derived from ground-based images. All SBPs have been corrected for extinction (A_V = 0.13 mag). The thick-grey line shows a linear fit to the B SBP for $R^* \geq 8''$. **b)** B SBP of I Zw 18 as obtained from ground-based data using: (1) concentric circular apertures centered on the NW region (filled points) and (2) ellipse fitting to the isophotes (triangles), without removal of compact sources in the LSB envelope (see discussion in the text). Dashed curves show the variation of the SBPs obtained with method (1) when the sky background is over- or underestimated by ±1 count. The linear fit to the LSB envelope in panel **a)** and the B SBP of Kunth & Östlin (2000) (open circles) are included for comparison. **c)** Overlay of ground-based B and R SBPs on *HST*/WFPC2 V (F555W) and R (F702W) SBPs. The solid line has the same meaning as in panel **a)**. **d)** Colour profiles obtained by subtraction of ground-based (panel **a)**) and *HST*/WFPC2 (panel **c)**) SBPs. Dotted lines indicate the average $B-R$ (denoted *1*) and $B-V$ (denoted *2*) colours obtained in the radius range $6'' \leq R^* \leq 12''$, using *HST*/WFPC2 images taken through the wide B (F450W) filter.

extrapolation of the B SBP slope to infinite radius, we obtain for the LSB envelope a total magnitude m_B = 17.7 mag (equivalent to ∼24% of the B light). With a distance modulus of −30.88 mag, this corresponds to an absolute magnitude $M_{\rm LSB}$ = −13.2 mag. An exponential slope is also seen in the J SBP for $\mu \gtrsim 23.5$ J mag/□″, though with a significantly smaller scale length ($\alpha \sim 165$ pc). Since our data does not allow for surface photometry beyond ∼25 J mag/□″, deeper imaging as that obtained by Hunt et al. (2002) is needed to assess the NIR properties of I Zw 18 in its outermost regions.

The smooth exponential decrease in the LSB outer parts of I Zw 18 is surprising in view of its filamentary morphology. We have checked that this is not an artifact introduced by methods iii) and iv). Figure 7b shows the overlay of the exponential

slope in panel a on ground-based B SBPs derived by: (1) flux averaging within concentric circular apertures centered on the NW region (filled circles), and (2) ellipse fitting to isophotes prior to the removal of contaminating sources (triangles). The dashed curves show the shift that an offset of ±1 count in the sky subtraction would introduce in the SBPs computed with method (1). We also show in Fig. 7b the B SBP of Kunth & Östlin (2000). All SBPs are in good agreement. Within the uncertainties, our derived B central surface brightness and scale length are consistent with $\mu_{E,0}$ = 22.9 mag/□″ and α = 310 pc read off Fig. 8 in Kunth & Östlin (2000). *HST* V (F555W) and R (F702W) SBPs are also nearly indistinguishable from ground-based profiles in B and R in the radius range $8'' \leq R^* \leq 14''$ (Fig. 7c). Thus, although α may vary by ∼20% depending on the profile extraction method, the LSB envelope of I Zw 18 can be well fitted by an exponential law, despite its patchiness.

Figure 8 shows that the B SBP of I Zw 18 resembles closely that of an evolved iE BCD, such as Mkn 178 or VII Zw 403. All three systems have similar isophotal sizes E_{25} and exponential scale lengths (∼0.25–0.37 kpc). Furthermore, the absolute magnitude of the LSB envelope of I Zw 18 ($M_{LSB} \approx -13.2$ mag) is comparable to that of Mkn 178 ($M_{LSB} \approx -13.1$ mag) and VII Zw 403 ($M_{LSB} \approx -13.2$ mag). The only notable difference between standard BCDs and I Zw 18 becoming apparent from Fig. 8 (bottom) is that the latter is considerably bluer throughout, the difference getting more pronounced in the outer regions.

The $B-R$ and $V-R$ colours of I Zw 18 (Fig. 7d) increase smoothly, with gradients 0.74 mag kpc^{-1} and 0.65 mag kpc^{-1} for radii $R^* \leq 9''$ (∼0.65 kpc). In the LSB regime ($\mu \geq 25.2$ B mag/□″) both profiles level off at $B-R \approx 0.55$ mag and $V-R \approx 0.47$ mag. The $B-R$ colour derived here is in good agreement with the value of ∼0.6 mag of Kunth & Östlin (2000).

Assuming that the LSB emission in I Zw 18 is predominantly stellar, the observed $B-R$ colour would translate into an age τ of at least a few hundred Myr. From the PEGASE.2 evolutionary synthesis models (Fioc & Rocca-Volmerange 1997) and adopting a Salpeter IMF with a lower and upper stellar mass limit of 0.1 and 120 $M_\odot$ and a stellar metallicity of $Z_\odot/50$, one infers for an instantaneously formed stellar population a $\tau \sim 0.8$ Gyr. For an exponentially decreasing SF rate with an e-folding time of 1 Gyr, τ increases to ∼2 Gyr, comparable to previous age estimates by Aloisi et al. (1999; 0.5–1.0 Gyr), Östlin (2000, ≥1 Gyr) and Kunth & Östlin (2000; ∼1–5 Gyr).

However, such an evolutionary scenario for I Zw 18 cannot account for all colours derived for the LSB envelope (Fig. 7d). The observed $V-R$ colour of 0.47 mag would require an age of ∼20 Gyr for a decreasing SF rate with an e-folding time of 1 Gyr. Such a $V-R$ colour has been observed for the LSB host of old more metal-rich BCDs, such as Mkn 5, Mkn 33, Mkn 35, Mkn 370 (Cairós et al. 2001a) and Mkn 86 (Gil de Paz et al. 2000). However, these systems also show red $B-V$, $B-R$ and $V-I$ colours equal to ∼0.5 mag, ≥1.0 mag and ∼0.9 mag, respectively, in contrast to the $B-V$ and $V-I$ colours of the LSB envelope of I Zw 18 which are both very blue, equal to ∼0.1 mag and ∼0 mag, respectively. For an exponentially decreasing SF, such colours would respectively translate into

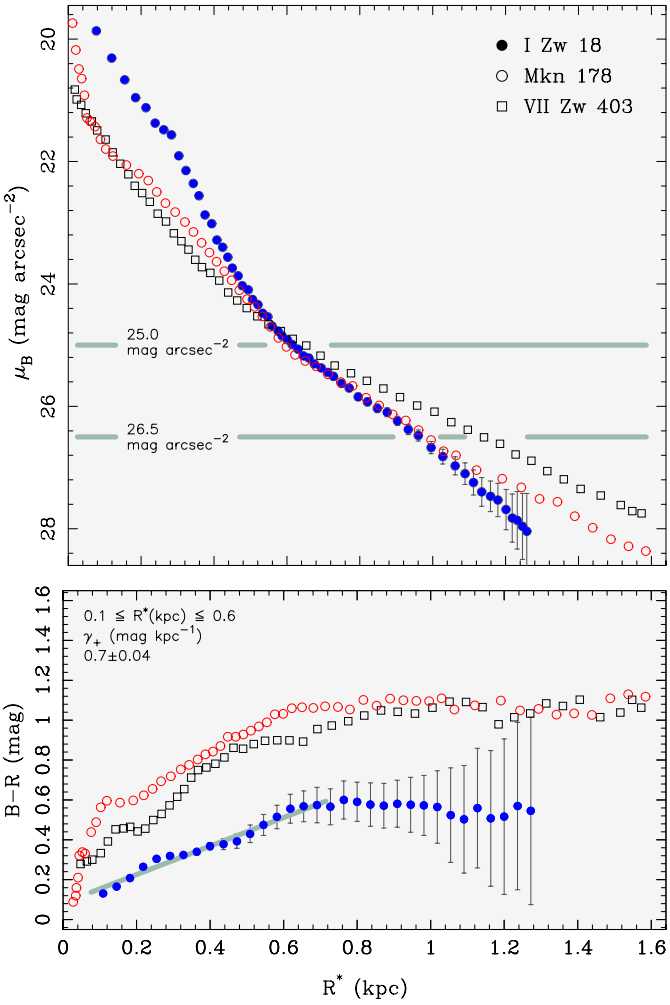

Fig. 8. (top) Comparison of the ground-based B SBP of I Zw 18 with those of Mkn 178 and VII Zw 403. All three BCDs have a similar E_{25} and Holmberg radius, and show for $R^* > 0.6$ kpc an exponential intensity decrease. The $B-R$ profile of I Zw 18 (bottom) shows for $R^* < 0.6$ kpc a linear colour increase with an average gradient $\gamma_+ \approx 0.7$ mag kpc^{-1}, similar to that derived for Mkn 178 in Sect. 3.1. I Zw 18 is bluer throughout in comparison to the standard BCDs, the difference in the $B-R$ colour exceeding 0.5 mag in the LSB regime, i.e. when $\mu > 25$ B mag/□″.

stellar ages of ∼0.8 Gyr and <100 Myr, much lower than those obtained before (an instantaneous burst model would result in even lower ages). As for the $B-J$ colour, its value of ∼0.6 mag at $R^* = 9''$ suggests a stellar age ≲250 Myr. Beyond that radius corresponding to $\mu \sim 25$ J mag/□″, noise and source confusion prevent a reliable determination of optical–NIR colours.

Since neither a relatively young stellar population formed instantaneously nor an older one formed through an exponentially declining SF process can simultaneously account for all observed LSB colours, it is to be expected that also a purely stellar emission connected with other schematic SF histories (e.g., constant SF, periodic bursts) will not allow for a consistent solution. Therefore we have to abandon in the case of I Zw 18 the usual assumption that stellar emission dominates the light of the LSB envelope of BCDs.

As noted in Sect. 3.1, the combination of blue $V-I$ (≲0 mag) with moderately red (∼0.3–0.6 mag) $B-R$ colours

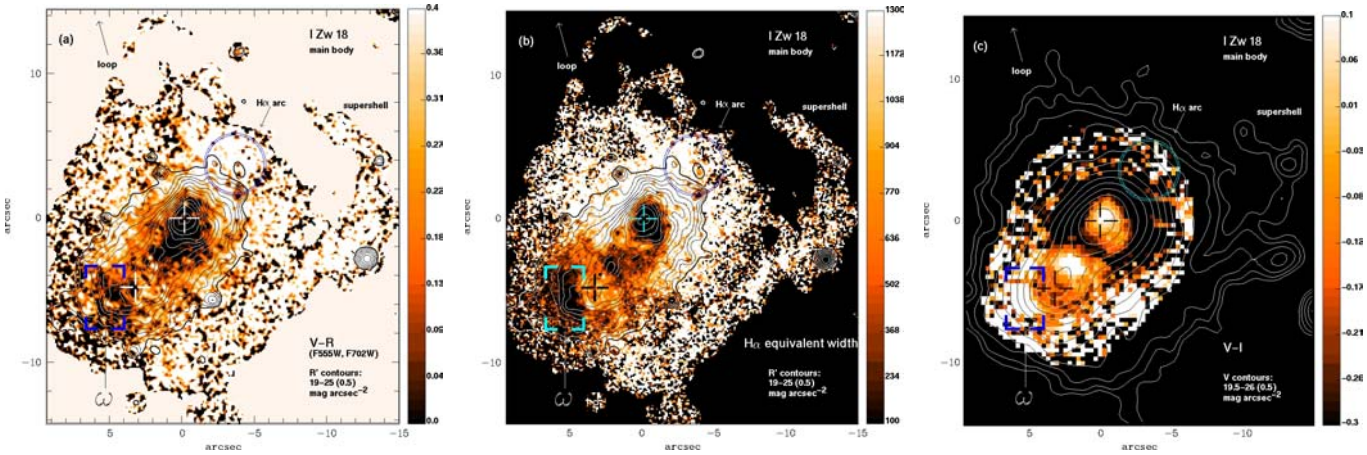

Fig. 9. a) $V-R$ map of I Zw 18, as derived from *HST*/WFPC2 F555W and F702W images, assuming a uniform extinction of $A_V = 0.13$ mag. Crosses mark the positions of the NW and SE star-forming regions. The region labelled "Hα *arc*" and the direction of the northern tip of the filamentary envelope ("*loop*"), discussed by Izotov et al. (2001a), are indicated. Contours show the morphology of the stellar and ionized gas continuum emission (referred to as R'), as obtained after subtraction of Hα emission from *HST*/WFPC2 F702W images. Contours go from 19 to 25 R' mag/□″ in steps of 0.5 mag. A relatively smooth stellar host (denoted LSB*, cf. Sect. 4.3) underlying the NW and SE regions, is seen. Note the featureless red ($V-R \gtrsim 0.4$ mag) envelope surrounding the stellar body beyond the 25 mag/□″ R' isophote. The southeastern tip of the LSB* component where ionized gas emission is negligible is labelled ω. **b)** Hα equivalent width (EW(Hα)) map of I Zw 18 in the range 100–1300 Å (cf. Izotov et al. 2001a). Contours have the same meaning as in panel **a)**. Note that the EW(Hα) increases sharply in the periphery of region NW, outside the 22 mag/□″ R' isophote, exceeding 1300 Å throughout the northwestern part of I Zw 18. **c)** $V-I$ map of I Zw 18, as derived from ground-based data. The colour map is displayed in the range –0.3–0.1 mag and overlaid with 19.5 to 26 mag/□″ V contours. Note that the morphology of the blue ($V-I \sim -0.5$ mag) region surrounding the NW component correlates well with the $V-R$ and EW(Hα) morphologies (panels **a)** and **b)**). The reddest $V-I$ colours are observed 3.″6 northwest and southeast of the SE region, both coinciding with local minima in the EW(Hα) distribution (cf. panel **b)**). The intermediate region, located between the SE and NW regions, shows $V-I \approx 0.1$ mag while $V-I$ in region ω ranges between 0.17 and 0.32 mag.

suggests a significant nebular line contamination. There are a few examples of BCDs with colours severely affected by ionized gas emission on a spatial scale comparable to the LSB envelope of I Zw 18, the magnitude of the effect depending on the telescope-filter transmittance and the spectroscopic properties and redshift of the BCD. One example is the starburst region of the BCD Tol 1214–277 with EW(Hβ) ≈ 324 Å, $U-B \sim -0.9$ mag and $B-R \sim 0.4$ mag (Fricke et al. 2001). Another is the filamentary LSB envelope of the BCD SBS 0335–052 E where ionized gas accounts for ∼1/3 of the optical emission (Izotov et al. 1997, 2001b). Just as in I Zw 18, the outer parts of SBS 0335–052 have a $B-R$ index of ∼0.7 mag together with very blue $U-B \sim -0.8$ and $V-I \sim -0.06$ mag (Thuan et al. 1997; Papaderos et al. 1998), a combination of colours which points to a substantial contribution of ionized gas emission.

The ionized gas emission hypothesis is also supported by the fact that the apparent magnitude of I Zw 18 as determined from *HST* images with the F450W B filter, $m_B = 15.83$ mag, is ∼0.3 mag brighter than $m_B = 16.12$ mag derived from ground-based Johnson B images. This is not the case for the *HST* F555W and ground-based Johnson V magnitudes which agree to within 0.02 mag. Contrary to Johnson B, the transmittance of the F450W filter at the Hβ and [O III]$\lambda\lambda$4959, 5007 wavelengths is comparable to that at 4300 Å, suggesting that the brighter F450W B magnitude is caused by prominent emission lines. Consequently, the $B-V = -0.23 \pm 0.06$ mag and $B-R = 0.14 \pm 0.04$ mag derived in the LSB envelope from the *HST* images (dotted lines *1* and *2* in Fig. 7d), are significantly bluer than those derived from ground-based images.

Recently, deep Keck spectra by Izotov et al. (2001a) have shown that nebular line emission is present as far as 30″ (∼2.2 kpc) from the main body of I Zw 18, and that the equivalent width of the Hα line exceeds 1300 Å over the whole northwestern half of the BCD and along the western supershell. In the regions labelled *loop* and Hα *arc* in Fig. 1 the EW(Hα) attains values of ≈1400 Å and ≈1700 Å, respectively (Izotov et al. 2001a). These results are in agreement with the high (∼1500 Å) EW(Hα) measured over a large part of the optical extent of I Zw 18 by Östlin et al. (1996) from high resolution ground-based images.

It is instructive to compare the $V-R$ and $V-I$ maps with the EW(Hα) distribution (Fig. 9). The reddest $V-R$ colours (0.2–0.5 mag) are observed along the supershell and the extended Hα rim intersecting the Hα *arc* region (Fig. 9a). On the other hand, the $V-I$ colours in the corresponding regions (panel c) show an opposite trend, being the bluest (∼–0.5 mag). Inspection of Fig. 9b reveals that extended regions showing both red $V-R$ and blue $V-I$ colours are spatially correlated with the EW(Hα), but are anticorrelated with the surface density of the stellar background (contours in panels a and b). This situation resembles that in the periphery of bright SF regions in VII Zw 403 (Sect. 3.1) or the one described by Fricke et al. (2001) in the BCD Tol 1214–277. In the absence of a significant underlying stellar component, the EW(Hα) in the extended ionized gas emission raises in the latter to ∼2000 Å as far out as 2.7 kpc away from the starburst region.

The conspicuous spatial anticorrelation between stellar and nebular emission together with the tight spatial coupling of

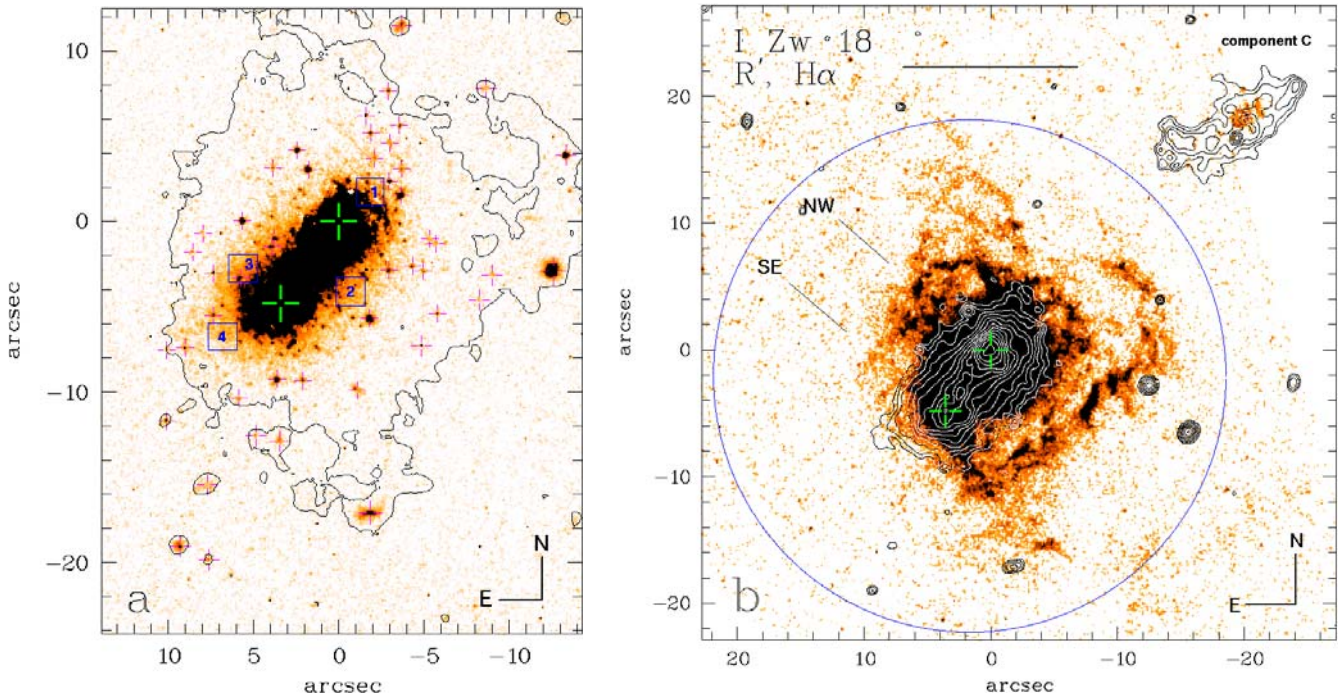

Fig. 10. a) R' map of I Zw 18. The contour shows the morphology of the BCD at 26 R mag/□″, prior to subtraction of Hα emission. Large crosses indicate the positions of the SE and NW star-forming regions. Small crosses mark the location of compact sources in the outer parts of I Zw 18 that have been removed before the derivation of surface brightness profiles (Figs. 5a, 5c and 11a). The mean $B' - V'$ colour decreases from ∼0.17 mag in region 1 to 0.05–0.1 mag in region 4 and inside the southeastern region ω (cf. Fig. 9). The $V' - R'$ colour is still significantly affected by ionized gas continuum emission in region 1 (∼0.3 mag), being ∼0.12–0.18 mag in the southeastern tip of I Zw 18. **b)** R' contours overlaid on an Hα map of I Zw 18, in the range 18.5 to 25.5 mag/□″ in steps of 0.5 mag. The circle, 40″ in diameter, is centered between the NW and SE regions.

EW(Hα) with colours renders a meaningful study of any stellar LSB background component of I Zw 18 from broad-band data impossible. Therefore it is necessary to subtract the ionized gas emission prior to the broad-band photometry.

4.2. Subtraction of nebular line emission

One way to subtract out the contribution of the line and continuum emission of the ionized gas is to use long-slit spectra (Papaderos et al. 1998; Thuan et al. 1999; Noeske et al. 2000; Izotov et al. 2001a; Guseva et al. 2001). However, this allows correction only along the slit position, i.e. it can hardly be used to study the 2-dimensional properties of the stellar LSB component in I Zw 18.

Therefore we decided to use continuum-subtracted narrow-band Hα and [O III] λ5007 maps to correct broad-band *HST* images for the strongest nebular emission lines. We first correct the R (F702W) image where Hα is the major contributor of ionized gas emission by subtracting from the R frame the continuum-subtracted Hα (F658N) image, scaled by a factor $c_R \approx 0.7$. The resulting image is called R' (Fig. 10a). The scaling factor has been determined by taking into account the telescope/detector throughput with the F658N and F702W filters at the redshifted wavelength of the Hα line, the respective exposure times and the width of the F702W filter. The latter has been calculated by integrating the system/filter transmittance curve over the wavelength range 5700 Å–9000 Å.

The subtraction of the Hα emission results in a nearly complete removal of the patchy LSB envelope of I Zw 18. While this correction has practically no effect on the C component (its flux is reduced by less than 2%), it removes about 1/3 of the R light in the main body. Some residual ionized continuum emission is still visible on the R' image, especially along the northwestern supershell. Since these faint (25.2 mag/□″ $\lesssim \mu_{R'} \lesssim$ 26.7 mag/□″) residuals are well separated from the main body and can be easily masked out before computing SBPs (Fig. 11a), no attempt has been made to remove them by adjusting c_R. A nearly complete subtraction of both the Hα and continuum emission was possible however, by decreasing c_R in small steps to about 0.5. Each resulting image was visually inspected after adaptive smoothing and checked for non-negative background. From the image with $c_R = 0.5$, we estimate the total ionized continuum and Hα contribution to be ∼50% of the R light of I Zw 18. The subtraction of the Hα emission gives the LSB component underlying the NW and SE SF regions of I Zw 18 a more regular and compact appearance (Fig. 10b, R' contours). The compactness of the stellar host galaxy can also be seen in Fig. 1c by Dufour et al. (1996b) who were the first to present *HST*/WFPC2 V images with the ionized gas emission removed.

Correction for nebular line emission is more uncertain for the B (F450W) and V (F555W) images, since both are contaminated by several prominent Balmer and oxygen emission lines. While e.g. the [O II]λ3727, Hδ, Hγ emission lines

are included in F450W only, both filters have nearly the same transmittance near the Hβ and [O III]$\lambda\lambda$4959, 5007. Because of the lack of complete 2-D information, we have taken the line ratios tabulated for the region "Hα *arc*" by Izotov et al. (2001a) to be representative for the whole LSB envelope.

First we determined for each filter the ratio of the flux $f_{\rm i}$ of the [O III] λ5007 line to the sum of the fluxes of all other prominent emission lines. In doing so, we have taken into account the intensity of each emission line and the system's transmittance at the corresponding redshifted wavelength. From each $f_{\rm i}$ and the estimated flux contribution of the [O III] λ5007 line to the filters F450W and F555W, we computed the factors c_B and c_V which we used to scale the F502N image prior to its subtraction from broad-band images. Alternatively, B and V images were corrected using both F502N and F658N exposures to subtract separately oxygen and Balmer emission lines. Visual inspection of the corrected images after adaptive filtering shows that both approaches give comparable results, with uncertainties in the SBP slope comparable to 1σ Poisson errors.

4.3. Surface photometry of the stellar and ionized gas continuum in the main body of I Zw 18

In the following we use broad-band *HST*/WFPC2 images, corrected for nebular line emission (henceforth denoted B', V' and R'), to compute the surface brightness and colour distribution of the *unresolved* LSB background surrounding the NW and SE regions. As in Sect. 3.1, we have first replaced compact sources in the outer parts of I Zw 18 (indicated by crosses in Fig. 10a) by the mean value of adjacent regions. We refer to the residual stellar and ionized continuum LSB emission of I Zw 18, obtained after subtraction of the nebular line contribution, as LSB*, in order to distinguish this from the filamentary LSB envelope studied from raw B, V and R images in Sect. 4.1.

In Fig. 11a we compare the B', V' and R' SBPs of I Zw 18 with its R SBP (Fig. 7c). The B', V' and R' profiles are nearly indistinguishable from one another, suggesting negligible colour gradients over the optical extent of the BCD. They display an exponential fall-off with a scale length $\alpha \sim 100$ pc for $R^* \gtrsim 3''$ (~0.2 kpc). To ensure that residual gaseous continuum emission in the vicinity of the SF regions does not affect the derived structural properties of the LSB* component, we fit only its outermost regions ($R^* \geq 0.5$ kpc) where the surface brightness drops in all bands to less than 25 mag/$\Box''$, and where in standard BCDs, the emission is dominated by the luminosity of the evolved stellar LSB host (cf. Sect. 3.2). Linear fits give in all bands $\alpha \sim 120$ pc and a B' central surface brightness $\mu_{\rm E,0} \approx 20.7$ mag/$\Box''$ (cf. Table 3). The dashed line in Fig. 11a represents the SBP of the LSB* component, estimated by fitting ellipses to the B' image, without masking out compact sources or spots of residual continuum emission along the northwestern supershell. Its scale length of 160 pc represents a formal upper limit to the true scale length of the LSB* component.

From the comparison of the R and R' SBPs (Figs. 7c and 11a), we can derive a one-dimensional representation of the relative contribution of the stellar and ionized gas continuum to the R intensity as a function of the galactocentric radius R^*. Figure 12 shows that the stellar and ionized gas continuum emission dominates only within the inner 0.2 kpc (~$r_{\rm eff}$; cf. Table 3) of I Zw 18. For larger radii, its contribution gradually decreases, becoming less than 20% at $R^* \sim 0.65$ kpc (9″). Beyond that radius, where the surface brightness is $\gtrsim$26 R' mag/$\Box''$, the data become too noisy to allow to pin down the line-of-sight contribution of the stellar component to the total luminosity. However, since nebular line emission accounts for at least 80% of the R flux at large radii, it determines the colour in the outer parts of I Zw 18 (cf. Fig. 7d).

The LSB* underlying component of I Zw 18 shows an important difference as compared to the main class of evolved BCDs. From both surface photometry and CMD studies, it is known that these systems show a substantial reddening from the SF region to the LSB periphery (Sect. 3.1). The $B' - V'$ and $V' - R'$ profiles of I Zw 18 (Fig. 11b) do show relatively strong gradients of respectively 0.72 ± 0.03 mag kpc^{-1} and 0.77 ± 0.05 mag kpc^{-1} within the inner ~0.2 kpc, only. However, at larger radii both colours remain blue ($B' - V' = 0.09 \pm 0.04$ mag and $V' - R' = 0.12 \pm 0.04$ mag), implying a minor colour contrast between the SF and the LSB* component. Because of this, subtraction of the LSB* emission (cf. Sect. 3.1) has practically no effect on the colour profile inside P_{25} (~0.3 kpc). This correction shifts the $B' - V'$ and $V' - R'$ colours at $R^* \approx 60$ pc to –0.07 mag and –0.03 mag, respectively, not significantly bluer than those obtained from direct SBP subtraction. This is to be compared with the situation for the old BCDs Mkn 178 and VII Zw 403 (Sect. 3.1, Figs. 5b and 5d), where correction for the red LSB background shifts optical colours by –0.4–−0.6 mag over a galactocentric distance of ~0.5 kpc.

Admittedly, surface photometry allows to derive only a luminosity-weighted average colour. By this fact, a nearly constant blue colour (Fig. 11b) over a surface brightness span of some 8 mag does not rule out *per se* the presence of a faint old stellar background. However, inspection of colour maps does not show any evidence for such a population. Even after subtraction of nebular line emission, the colours of I Zw 18 in its northern half, especially along the Hα *arc* ($B' - V' \approx 0.16$ mag, $V' - R' \approx 0.3$ mag) appear to be significantly affected by ionized continuum emission for which $B - V = 0.34$ mag and $V - R = 0.64$ mag (Krüger 1992). Towards the southeastern tip of I Zw 18, however, where, from the EW(Hα) map (Fig. 9b), ionized gas emission is weak, both colours become progressively bluer. In regions 3 and 4 (Fig. 10a) and throughout the southeastern tip of the LSB* body (region ω in Fig. 9), the $B' - V'$ and $V' - R'$ colours decrease to ~0.05–0.1 mag and 0.12–0.18 mag, respectively.

At the same time, region ω is identifiable with the reddest part of the LSB* host with respect to the $V - I$ colour (cf. Fig. 9c), determined to be 0.17…0.32 mag. Thus, the LSB* component of I Zw 18 in its southeastern tip is by ~0.3 mag redder than the ionized envelope regarding its $V - I$ colour (Fig. 7d). It is, however, ~0.6 mag bluer than the LSB component of normal BCDs, such as VII Zw 403 (Fig. 5d) or that of the nE BCD Mkn 996 (Thuan et al. 1995).

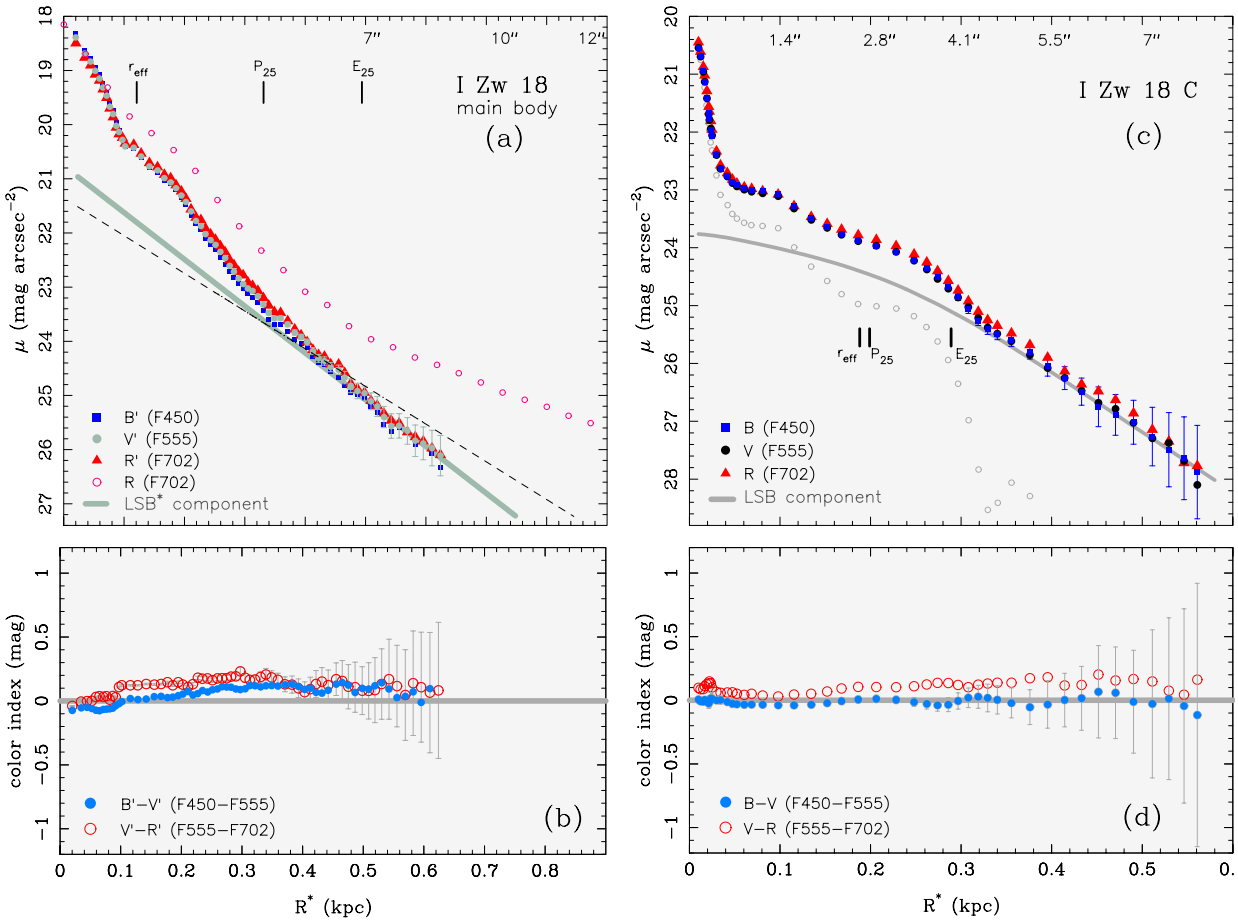

Fig. 11. a) Surface brightness profiles of the main body of I Zw 18 derived from archival *HST*/WFPC2 *B* (F450W), *V* (F555W) and *R* (F702W) images, after subtraction of nebular line emission. These SBPs, labelled B', $V'$and R', show the radial intensity distribution of the stellar and ionized gas continuum emission. For comparison, we show with open circles the *R* SBP, as derived prior to subtraction of nebular line emission (Fig. 7c). A linear fit to the outermost part ($R^* \geq 0.5$ kpc) of the V' SBP (labelled "LSB* component") is shown by the thick-grey line. The slope of the dashed line is an upper limit to the exponential scale length of the LSB* component. It has been derived from fitting ellipses to its outer parts, without removing isolated spots of residual ionized continuum emission along the northwestern supershell. The effective radius $r_{\rm eff}$ and the isophotal radii P_{25} and E_{25} of the star-forming and LSB components at 25 *V* mag/□″ are indicated. **b)** $B' - V'$ and $V' - R'$ colour profiles of the main body of I Zw 18, obtained by subtraction of the SBPs in panel **a)**. **c)** SBPs of I Zw 18 C derived from archival *HST*/WFPC2 images assuming $A_V = 0$ mag. The thick grey curve (labelled "LSB component") shows a model of the *B* intensity distribution of the LSB component, according to Eq. (2) with $(b, q) = (2.4, 0.8)$. The surface brightness distribution of the luminosity in excess of the fit is shown by small open circles. The radii $r_{\rm eff}$, P_{25} and E_{25} refer to the *B* SBP. **d)** $B - V$ and $V - R$ colour profiles of the C component.

In summary, the *unresolved* LSB* host of I Zw 18 which is well approximated by the colour profiles in Fig. 11b has significantly bluer colours than in standard evolved BCDs.

4.4. The C component

Before we proceed to the discussion of the implications of our photometric analysis for the evolutionary state of I Zw 18 we briefly discuss the photometric structure of the faint northwestern component I Zw 18 C. Surface brightness profiles for this system (Fig. 11c) were derived from *HST*/WFPC2 *B*, *V* and *R* exposures after removal of compact sources in its periphery (Sect. 4.3). Figure 11c shows that the faint (>26 *B* mag/□″) outer parts of its LSB component are well fitted by an exponential law. However, profile extrapolation to the center results in a higher intensity than is observed in the radius range $0.05 \lesssim R^*$ (kpc) $\lesssim 0.2$, implying a significant flattening of the exponential profile inside ∼0.3 kpc. This type of convex profile has frequently been reported for early- and late-type dwarfs (Vennik et al. 2000; Guseva et al. 2001 and references therein). Such a distribution can be approximated by a Sérsic profile with an exponent $\eta > 1$ (e.g. Caon et al. 1993; Cellone et al. 1994) and an exponential distribution flattening inwards, such as the one proposed in P96a:

$$I(R^*) = I_0 \exp\left(-\frac{R^*}{\alpha}\right)\Big[1 - q \exp(-P_3(R^*))\Big], \quad (2)$$

where $P_3(R^*)$ is

$$P_3(R^*) = \left(\frac{R^*}{b\,\alpha}\right)^3 + \left(\frac{R^*}{\alpha}\,\frac{1-q}{q}\right). \quad (3)$$

Near the center, the intensity distribution (Eq. (2)) depends on the relative central intensity depression $q = \Delta I / I_0$, where I_0 is the central intensity obtained by extrapolation to $R^* = 0$ of

Table 3. Structural properties of I Zw 18 (main body) and I Zw 18 C[a].

Component	Band	$\mu_{E,0}$	α	$m_{\rm LSB}^{\rm fit}$	P_{25}	$m_{P_{25}}$	E_{25}	$m_{E_{25}}$	$m_{\rm SBP}$	$m_{\rm tot}$	$r_{\rm eff}$, r_{80}
		mag/□″	pc	mag	pc	mag	pc	mag	mag	mag	pc
(1)	(2)	(3)	(4)	(5)	(6)	(7)	(8)	(9)	(10)	(11)	(12)
I Zw 18	B	22.33 ± 0.14	249 ± 10	17.67	468	16.44	611	18.05	16.11 ± 0.01	16.12[b]	200, 344
main body	V	22.23 ± 0.17	246 ± 16	17.59	469	16.29	627	17.91	16.01 ± 0.01	16.01	181, 319
ground-based	R	21.71 ± 0.17	244 ± 12	17.08	462	16.33	741	17.31	15.90 ± 0.02	15.89	220, 377
	I	22.28 ± 0.24	247 ± 27	17.63	471	16.33	619	18.00	16.04 ± 0.03	16.00	174, 323
	J	20.41 ± 0.60	165 ± 39	16.64	409	16.45	697	16.73	15.83 ± 0.13	15.80	180, 311
I Zw 18	B'	20.72 ± 0.23	123 ± 6	17.58	323	16.88	485	17.69	16.43 ± 0.02	16.42	114, 221
main body	V'	20.73 ± 0.13	126 ± 4	17.55	331	16.90	494	17.66	16.42 ± 0.03	16.40	121, 230
HST	R'	20.50 ± 0.16	123 ± 9	17.37	343	16.82	509	17.46	16.31 ± 0.02	16.31	129, 240
I Zw 18[c]	B	22.01 ± 0.22	105 ± 4	19.22	199	20.52	289	20.19	19.18 ± 0.05	19.19	188, 298
C component	V	21.99 ± 0.27	105 ± 6	19.19	187	20.64	292	20.15	19.19 ± 0.06	19.20	189, 300
HST	R	21.73 ± 0.31	103 ± 8	18.98	159	20.88	310	19.85	19.1 ± 0.05	19.08	193, 305

[a] A distance of 15 Mpc has been adopted for I Zw 18 (Izotov et al. 2001a). The tabulated values assume an extinction $A_V = 0.13$ mag for I Zw 18 and no extinction for the C component.
[b] The B magnitude, as obtained from *HST*/WFPC2 F450W images is 15.83 mag, nearly 0.3 mag brighter than the magnitude derived from ground-based Johnson B images.
[c] The intensity distribution of the LSB component of I Zw 18 C has been modelled adopting an exponential distribution which flattens inward (Eq. (2)) with $(b, q) = (2.4, 0.8)$. Note that this model implies for the LSB component a total magnitude 0.5 mag fainter than the integrated magnitude of a purely exponential distribution (Col. 5).

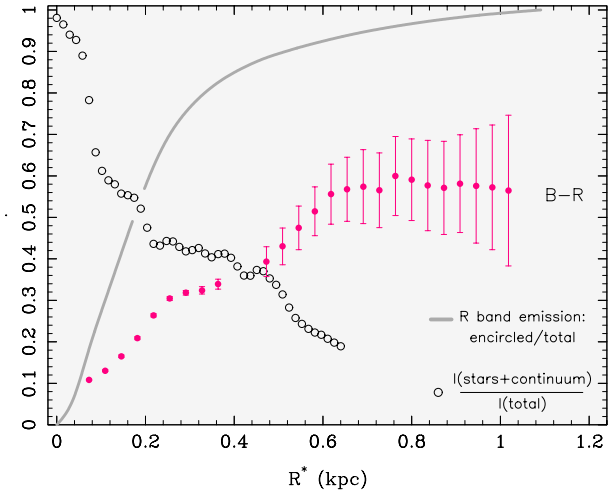

Fig. 12. Fractional contribution of the stellar and ionized gas continuum (R') to the R emission of the main body of I Zw 18 as a function of the galactocentric distance R^* (open circles). The run of the ratio of the luminosity within a circle of radius R^* to the total luminosity is shown by the light curve. The contribution of the underlying stellar component drops to <50% beyond the effective radius (~0.2 kpc, cf. Table 3). For $R^* > 0.65$ kpc (≈9″), ionized gas emission accounts for more than 80% of the R line-of-sight intensity and is responsible for the relatively red $B - R$ colour of the filamentary LSB envelope of I Zw 18 (cf. Fig. 7d).

the outer exponential slope with scale length α, and $b\alpha$ is the cut-off radius inside which the flattening occurs.

Following the procedure described in Guseva et al. (2001), we fitted Eq. (2) to the SBPs of I Zw 18 C for $R^* \geq 0.33$ kpc adopting $b = 2.4$ and $q = 0.8$. This fit (grey curve in Fig. 11c) gives for the LSB population an absolute B magnitude of −11.15 mag and $\alpha \sim 100$ pc, close to the scale-length obtained in Sect. 4.3 for the main body.

Figure 11d shows that, for $R^* \geq 0.2$ kpc, the mean $B-V$ and $V-R$ colours are respectively 0 ± 0.04 mag and 0.1 ± 0.04 mag. Because of its compactness, the radial colour distribution of component C cannot be derived from the available ground-based data. We measured a global $V - I$ colour of 0.12 mag for the C component, in good agreement with the value of 0.1 mag of van Zee et al. (1998b). As noted in Izotov et al. (2001a), I Zw 18 C shows a conspicuous colour gradient along its major axis, becoming markedly bluer from its northwestern tip ($B - V = 0.05$ mag, $V - I = 0.2$ mag) to its southeastern tip ($B - V = -0.07$ mag and $V - I = -0.2$ mag).

5. Discussion

5.1. The structural properties of the stellar LSB component in I Zw 18

In Fig. 13 we compare the absolute B magnitude $M_{\rm LSB}$, the central surface brightness $\mu_{\rm E,0}$ (panel a) and the exponential scale length α (panel b) of the LSB component of different types of dwarf galaxies. I Zw 18 is nearly indistinguishable from Mkn 178 and VII Zw 403 in the $\mu_{\rm E,0} - \alpha$ plane prior to subtraction of ionized gas emission. All three systems lie in the intermediate zone between the regions populated by dIs and iE/nE BCDs. However, subtraction of nebular line emission shifts I Zw 18 by –1.6 mag and –0.31 dex in panels a and b, respectively. Note that the absolute B magnitude of the stellar LSB* host (–13.3 mag) is close to the value derived for the patchy envelope (–13.2 mag) prior to subtraction of nebular line emission (Sect. 4.1). This is because, although the LSB* component is smaller by a factor ~2 in α, it is brighter by ≈1.6 mag in $\mu_{\rm E,0}$. As for I Zw 18 C, despite a difference

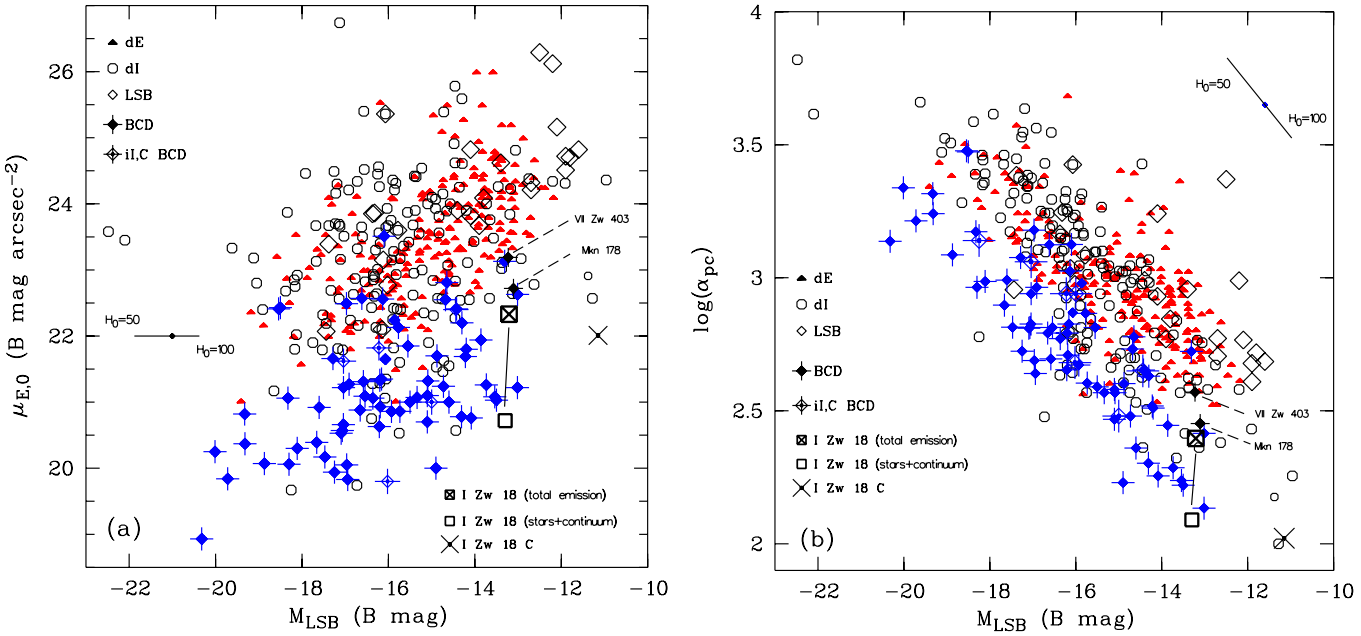

Fig. 13. Comparison of the structural properties of the stellar LSB component of BCDs with those of other types of dwarf galaxies. Data for iE/nE BCDs are compiled from Cairós et al. (2001a), Drinkwater & Hardy (1991), Marlowe et al. (1997), Noeske (1999), Noeske et al. (2002) and P96a, and for *cometary* iI,C BCDs from Noeske et al. (2000). Data for other types of dwarf galaxies (dE, dI and LSB) are taken from Binggeli & Cameron (1991, 1993), Bothun et al. (1991), Caldwell & Bothun (1987), Carignan & Beaulieu (1989), Hopp & Schulte–Ladbeck (1991), Patterson & Thuan (1996), Vigroux et al. (1986) and van Zee (2000). The horizontal line shows the shift of the data points caused by a change of the Hubble constant from 75 to 50 and 100 km s^{-1} Mpc^{-1}. **a)** Central surface brightness $\mu_{E,0}$ vs. absolute B magnitude M_{LSB} of the LSB component. **b)** Logarithm of the exponential scale length α in pc vs. M_{LSB}. Without correction for nebular line emission, I Zw 18 is located close to Mkn 178 and VII Zw 403 (Sect. 3.1), between the regions populated by iE/nE BCDs and other types of dwarf galaxies. Subtraction of nebular line emission shifts I Zw 18 by −1.6 mag and –0.31 dex in panels **a)** and **b)**, making it one of the most compact BCD known. The absolute B magnitude of the LSB component of I Zw 18 C (–11.15 mag) has been determined by extrapolating the fitting formula Eq. (2) to infinity. Note that the actual central surface brightness of I Zw 18 C, as given by Eq. (2) is ≈1.75 mag fainter than the extrapolated value $\mu_{E,0} \approx 22$ B mag/□″.

~2 mag in M_{LSB}, it is comparably compact ($\alpha \approx 100$ pc) as the main body. Thus, for $R^* \gtrsim 3\alpha$ the main body and the C component of I Zw 18 are very similar with respect to both the surface brightness distribution and the mean colour of their stellar LSB host galaxy (Figs. 11b and 11d).

As evident from Fig. 13, the LSB* component of I Zw 18 does not show exceptional structural properties as compared to other intrinsically faint dwarf galaxies. It does not have an unusually bright $\mu_{E,0}$ or an extraordinarily small α. This conclusion still holds even if the commonly assumed distance of 10 Mpc to I Zw 18 is adopted (Hunter & Thronson 1995; Dufour et al. 1996b; Aloisi et al. 1999). Assuming such a distance would merely result in a shift of 0.88 mag in M_{LSB} and of –0.18 dex in $\log\alpha$. Note that there are a few dIs in Fig. 13 that are as compact as I Zw 18 and I Zw 18 C regarding their exponential scale length. Examples are UGC 8091 (Patterson & Thuan 1996), DDO 210 (van Zee 2000) and UGC 5272 B (Hopp & Schulte-Ladbeck 1991). The BCD HS 0822+3542 ($\alpha \approx 85$ pc, Kniazev et al. 2000), the Ursa Minor and Leo I dwarfs in the Local Group ($\alpha \gtrsim 100$ pc, Caldwell et al. 1992) and a number of compact ($\alpha \sim 100$ pc) dwarfs in the Fornax Cluster (Hilker et al. 1999; Phillips et al. 2001; Drinkwater et al. 2001) have also a comparable scale length.

The archival *HST* images, after subtraction of nebular line emission (Sect. 4.2), do not go deep enough to allow to directly test the hypothesis of a faint ($\overline{\mu}_V \sim 28$ mag/□″) and extended stellar disc, forming in I Zw 18 continuously over a Hubble time (Legrand 2000). From its predicted magnitude ($m_V \sim 20$ mag, or ~10% of the LSB* light), and assuming that at least half of its mass is confined within 22″ from the main body of I Zw 18 (the angular distance between the NW region and the southeastern tip of I Zw 18 C), we deduce an upper limit $\alpha_{max} \lesssim 13''$ for its exponential scale length. Such a putative disc would escape detection at the outermost point of our SBPs ($\mu = 26.2 \pm 0.4$ V mag/□″ at $R^* = 8\farcs6$) at the 1σ level if its central surface brightness $\mu_{E,0} > 27.1$ mag/□″ and its scale length $\alpha > 10\farcs5$.

While the postulated disc can neither be confirmed nor ruled out with the present data, its stability over a Hubble time, in the presence of I Zw 18 C, has yet to be demonstrated by numerical simulations. Moreover, the disc hypothesis does not appear to be in accord with recent CMD studies. The few red ($V - I \geq 1$ mag) point sources detected in I Zw 18 (Aloisi et al. 1999) are all located within the LSB* host (Izotov & Thuan 2002). This is in contrast with CMD studies of standard BCDs which, in agreement with surface photometry, reveal a sizeable population of old stars lying well beyond the plateau radius P_{25} (Sect. 3.1). As the detectability of a point source above the photon noise decreases with the square root of the local intensity level, evolved stars would be traceable, if present, in the

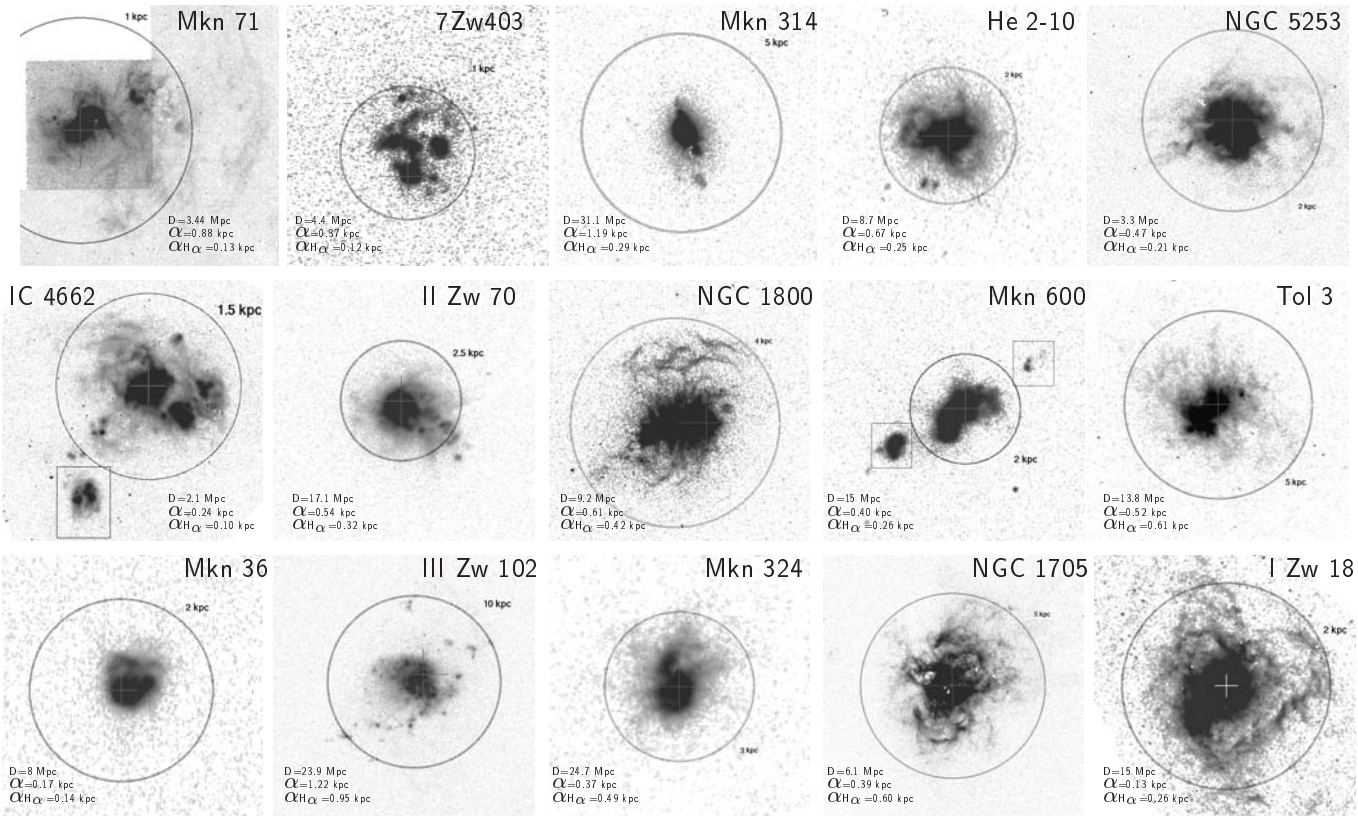

Fig. 14. Continuum-subtracted Hα images of a sample of nearby BCDs, the Hα surface brightness profiles of which are shown in Fig. 15. Each sample galaxy is labelled with the adopted distance and the B exponential scale length α of its stellar LSB host. $\alpha_{\mathrm{H}\alpha}$ is the scale length of the outer exponential part of the corresponding Hα profile. Each circle is labelled with its diameter in kpc.

periphery ($\mu > 27$ mag/□″) of the hypothetical disc rather than in front of the by two orders of magnitude brighter ($\mu < 22$ mag/□″) background in the central part of the LSB* host. The observed concentration of red point sources toward the center of I Zw 18 suggests that their red colours are not due to a large age. Hunt et al. (2002) have argued that these sources may be red supergiants or H II regions reddened by dust.

5.2. The ionized gas component of I Zw 18

We have seen that ionized gas emission dominates the light of I Zw 18 for $R^* > 0.2$ kpc (Fig. 12), and that its intensity falls off exponentially in the radius range $0.6 \lesssim R^*$ (kpc) $\lesssim 1.3$ (Figs. 7a and 7c). We wish to explore here whether this exponential fall-off is particular to I Zw 18 or it is a common property of the ionized halo of BCDs on scales of several kpc away from the SF region.

We have examined the Hα surface brightness profiles of a small sample of BCDs. The profiles were derived from continuum-subtracted Hα images (Fig. 14), based partly on data taken with the Danish 1.54 m telescope at La Silla (Papaderos & Fricke 1999; Noeske et al. 2002). The La Silla sample includes the BCDs He 2-10, NGC 5253 and the BCD/dI IC 4662. We have also used archival Hα images of the BCDs Tol 3 (ESO/NTT, PI: Vacca, Program 53.1-0086), NGC 1705 and NGC 1800 (ESO/VLT, PI: Tüllmann, Program 64.N-0399A; cf. Bomans 2001), as well as *HST*/WFPC2 narrow-band images of the H II region Mkn 71 in the nearby galaxy NGC 2366 (Noeske et al. 2000 and references therein). In addition, we included Hα images for VII Zw 403 (Sect. 3.1) as well as for a subset of objects in Cairós et al. (2001b), consisting of Mkn 36, Mkn 314, Mkn 324, Mkn 600, III Zw 102 and II Zw 70. The Hα images are shown in Fig. 14, each labelled with the adopted distance to the BCD and the B exponential scale length α of its stellar LSB component, taken from Cairós et al. (2001b) for Mkn 36, Mkn 314, Mkn 324, Mkn 600, III Zw 102, II Zw 70, from Marlowe et al. (1997) for NGC 1705, NGC 1800, from Noeske et al. (2000) for Mkn 71, from Papaderos & Fricke (1999) for He 2-10, from Noeske et al. (2002) for NGC 5253, Tol 3, IC 4662 and from Table 2 for VII Zw 403.

In Fig. 15 we plot the Hα surface brightness distribution of each BCD, shifted vertically by an arbitrary value, versus the equivalent radius $R^*_{\mathrm{H}\alpha}$ of the Hα emission, normalized to the scale length α. SBPs were derived using method iv) (large filled circles) and concentric circular apertures centered on the intensity maximum in each Hα image (small interconnected circles). We apply also the latter relatively crude technique to make sure that the derived SBP slope does not depend sensitively on the profile extraction method. The SBPs were derived from the total Hα emission, without distinguishing between emission from HSB H II regions and from the diffuse ionized medium. Note that the Hα profiles of Mkn 600 do not include the detached Hα sources indicated

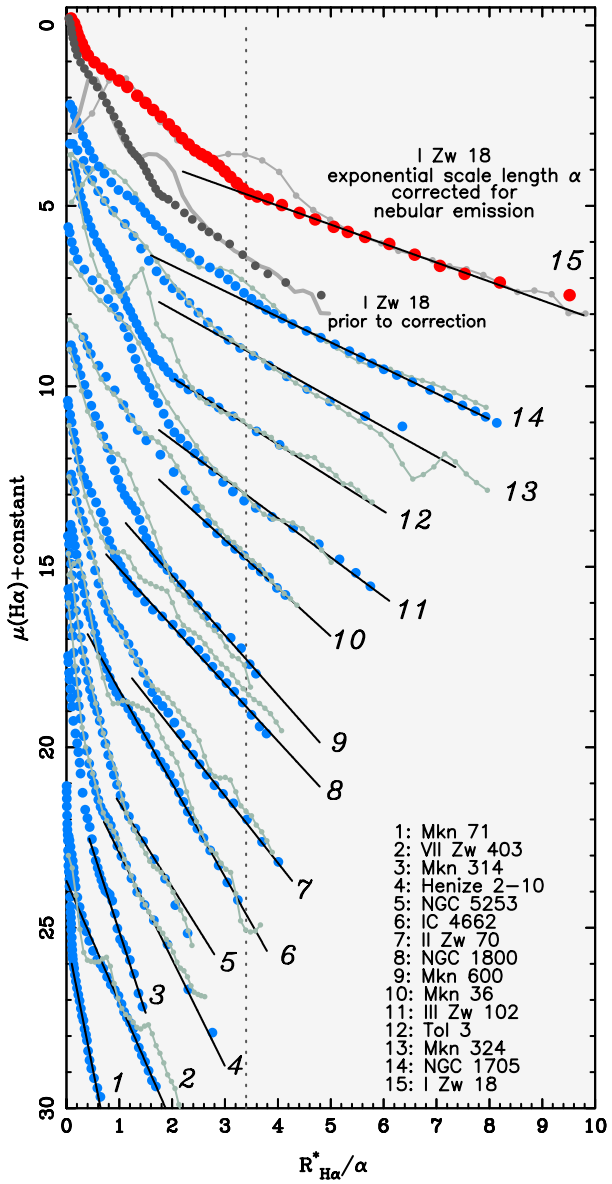

Fig. 15. Hα surface brightness profiles of the BCDs shown in Fig. 14, derived with method iv) (large filled symbols) and with concentric circular apertures (small interconnected symbols). The profiles have been shifted vertically by an arbitrary amount for clarity. The Hα surface brightness μ(Hα) is plotted against $R^*_{\rm H\alpha}/\alpha$ where $R^*_{\rm H\alpha}$ is the equivalent radius of the Hα light and α is the B exponential scale length of the stellar LSB component. For I Zw 18, the Hα profile with $R^*_{\rm H\alpha}/\alpha$ obtained from the scale length of the profile of the LSB envelope, prior to correction for nebular line emission is also included for comparison. Linear fits to the outer exponential part of each SBP are shown by black lines. The vertical dotted line indicates the mean E_{25}/α ratio of 3.4 ± 0.14 derived by Papaderos et al. (1996b) for a sample of evolved BCDs.

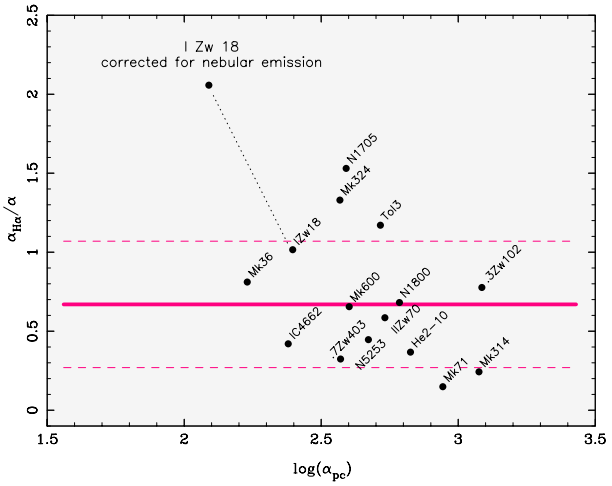

Fig. 16. Ratio of the exponential scale length $\alpha_{\rm H\alpha}$ of the outer parts of the Hα profiles (Fig. 15) to the B exponential scale length α of the stellar LSB component for the BCDs shown in Fig. 14. The thick line indicates the mean $\alpha_{\rm H\alpha}/\alpha$ ratio of 0.67 ± 0.4 derived for all sample BCDs, excluding I Zw 18. Dashed lines show the 1σ lower and upper bounds. Correction for nebular line emission pushes I Zw 18 upwards to a $\alpha_{\rm H\alpha}/\alpha$ ratio of 2.06.

by rectangles in Fig. 14. Furthermore, in computing the Hα profiles of IC 4662, we have excluded region d (Heydari-Malayeri et al. 1990; see also Hidalgo-Gamez et al. 2001) ∼1′ southwest of the galaxy (rectangle in Fig. 14).

From Fig. 15 it is evident that the Hα surface brightness profiles show for all sample galaxies a nearly exponential regime in the outer parts, typically at surface brightness levels fainter by ≳5 mag than the Hα maximum. The galactocentric radius where the exponential behaviour appears shows no dependence on the structural properties of the LSB galaxy, ranging from <1α in VII Zw 403 to ∼4α in NGC 1705. Given an average E_{25}/α ratio of ∼3.4 for BCDs (Papaderos et al. 1996b) where E_{25} is the isophotal radius at a surface brightness level of 25 mag/□″, our sample (Fig. 15) includes quite a few systems where the exponential Hα slope continues well beyond the optical size of the stellar LSB component. The most extreme case is NGC 1705 where deep VLT data allow us to trace the exponential intensity fall-off of its ionized gas halo out to ∼8α (3.1 kpc), or more than twice its isophotal radius E_{25}, in agreement with the Hα extent of ∼2 kpc found by Meurer et al. (1992) for this galaxy.

Figure 16 reveals that the scale length of the ionized halo $\alpha_{\rm H\alpha}$ (0.1–1 kpc) does not depend on the scale length of the stellar LSB host. Excluding I Zw 18, we obtain a mean $\alpha_{\rm H\alpha}/\alpha$ ratio of 0.67 ± 0.4 (thick gray line in Fig. 16), implying that the Hα intensity decreases in the outer regions of BCDs more steeply than the stellar light. This fact suggests that ionized gas contamination is generally of no concern in surface photometry studies of the LSB component of standard BCDs.

This *may* not be the case, however, in BCDs with $\alpha_{\rm H\alpha} \gtrsim \alpha$, i.e. for those systems located close to the line representing the 1σ upper bound in Fig. 16. I Zw 18 falls into that category. We obtain for it, prior to subtraction of nebular line emission, $\alpha_{\rm H\alpha}$ = 253 ± 10 pc, i.e. $\alpha_{\rm H\alpha}/\alpha \approx 1$ (cf. Table 3). Adopting the actual scale length of the stellar LSB* host (α = 123 pc) doubles the $\alpha_{\rm H\alpha}/\alpha$ ratio, shifting I Zw 18 to the upper left corner of Fig. 16.

The cursory study here suggests that an exponential intensity distribution may evolve in the warm ISM in the presence of SF activity on both, small and large spatial scales. Kennicutt (1984) has remarked that the emission measure of individual

H II regions follows a scalable exponential profile. This was found to also approximate well the surface brightness profiles of H II regions in nearby face-on galaxies (Rozas et al. 1988) and of the Hα halo of several Markarian starburst galaxies (Chitre & Joshi 2001).

From the evidence of Sect. 3, it appears that extended ionized emission in BCDs does not imply significant star formation beyond the E_{25} radius, although detached SF regions may exist at the periphery of these systems (Mkn 600, Cairós et al. 2001b; IC 4662, Hidalgo-Gamez et al. 2001; He 2-10, Beck & Kovo 1999). Instead, the exponential Hα distribution traceable to several kpc away from the SF region, is probably the result of the radiative and mechanical output of the starburst into the ambient ISM. As such, it deserves a closer study, since the Hα extent and its scale length $\alpha_{\mathrm{H}\alpha}$ may give clues to the amplitude and temporal progression of SF activity in BCDs.

As for I Zw 18, its exponential Hα envelope is not exceptional for BCDs, either by its extent or scale length. The central point is that I Zw 18 does not differ from standard BCDs in the properties of its ionized gas halo, but in its abnormally large $\alpha_{\mathrm{H}\alpha}/\alpha$ ratio. In the absence of an appreciable stellar underlying component, ionized gas emission dominates entirely in the periphery of I Zw 18, and its exponential profile mimicks that of a moderately red ($B-R\sim 0.6$ mag) stellar disc in optical SBPs. This has led some previous investigators to conclude erroneously that an evolved stellar disc exists in I Zw 18. Complementing optical photometry with $V-I$ or $B-I$ colours (see the discussion in Sect. 3; Izotov et al. 2001a) is essential for assessing the importance of ionized gas emission in the periphery of I Zw 18.

The case of I Zw 18 suggests caution in the search of more distant young galaxy candidates. Intense SF activity in the early phase of dwarf galaxy formation may result in an extended ionized gas halo which can be mistaken for an evolved stellar disc by studying only its exponential SBP.

5.3. Clues to the evolutionary state of I Zw 18

We have seen in Sect. 4.2 that subtraction of nebular line emission reveals a stellar host galaxy extending slightly beyond the SF region. The structural properties and formation history of this underlying population are central to the age debate of I Zw 18. Its blue colours are consistent with either the superposition of a young stellar population on an underlying old stellar LSB host, or a moderately young stellar population formed instantaneously or over an extended time period.

In the first scenario, the light of the old host galaxy is swamped by the light of an evenly distributed young ~100 Myr stellar population. By definition, photometry cannot disprove the presence of a massive though faint old stellar substrate down to an arbitrarily low mass limit, since the latter would cause a barely detectable colour shift. For instance, Papaderos et al. (1998) have argued that a 10 Gyr old population making up to 90% of the stellar mass may be present within the blue ($V-I\approx 0$ mag) LSB envelope of the metal-poor BCD SBS 0335–052 E. While such an old population cannot be entirely ruled out on photometric grounds (see also Vanzi et al. 2000), there is as yet no compelling reason to be postulated either.

In some BCDs a range of star-formation histories (SFHs) with very different mass fractions of young-to-old stars can account equally well for the observed colours, equivalent widths of Balmer absorption lines and spectral energy distributions. For instance, population synthesis models by Guseva et al. (2001) show that the above properties of the main body of the *cometary* iI BCD SBS 0940+544 can be well reproduced either by a young stellar population forming continuously since less than 100 Myr ago, or by an old stellar population which started to form 10 Gyr ago. In the latter case, however, the SFR over the last 100 Myr must have increased by a factor β of at least five. Likewise, in the case of I Zw 18, it is conceivable that a ratio of recent-to-past star formation rate $\beta > 1$ (cf. Guseva et al. 2001) may adequately explain its blue LSB* colours (Fig. 11b). Enhanced SF activity on a radial extent of ~0.65 kpc does not contradict empirical evidence for BCDs (Sect. 3); the LSB* host of I Zw 18 is comparable in size to the plateau component of standard BCDs, where photometric signatures of a diffuse and relatively young stellar population are present (cf. Sect. 3.1).

If this was the case, however, the ratio β must have been remarkably constant throughout the LSB* component, so as to eliminate any colour gradient. A constant β would imply that the amplitude of recent star formation is directly proportional to the surface density of the underlying old stellar background. Although there is empirical evidence that the structural properties of the stellar LSB host influence the global SF process in BCDs and dIs (cf. Sect. 3.2), such a tight spatial coupling between the old and young stellar populations does not seem plausible. From these considerations and lacking solid photometric evidence for a red stellar LSB envelope usually seen in standard BCDs for $\mu \gtrsim 25$ B mag/$\Box''$, we do not consider models with a dominant old host galaxy for I Zw 18.

Alternatively, if the LSB* component has formed in a single, instantaneous or extended SF episode, then its blue mean colours (Fig. 11b) are consistent with an age not greater than a few 100 Myr. The colours of the stellar LSB* population can be most reliably deduced from region ω (Fig. 9b), where the contribution of ionized gas emission is negligible. The colours $B'-V'=0.05$–0.08 mag, $V'-R'=0.12$–0.18 mag, and $V-I=0.17$–0.32 mag of this region translate for an instantaneously formed stellar population with the model assumptions described in Sect. 4.1 to an age of ~100 Myr. The age increases to $\lesssim$0.5 Gyr for a constant or exponentially decreasing SF model with an e-folding time $\tau=1$ Gyr, still considerably lower than the ages derived for standard iE/nE BCDs.

Similar considerations give for I Zw 18 C an age lower than or approximately equal to the age of the main body. The optical colours of the northwestern tip of I Zw 18 C ($B-V=0.05$ mag, $V-R=0.12$ mag, $V-I=0.2$ mag) are comparable to those of region ω. The limiting cases of an instantaneous burst and of a continuous SF give stellar ages between $\lesssim$100 and 350 Myr. Such estimates are consistent with the upper age limit of 100 Myr derived recently for I Zw 18 C by Izotov et al. (2001a), based on its broad-band colours, the equivalent

width of Balmer emission and absorption lines and the spectral energy distribution of its stellar continuum. To summarize, simple SFHs do not indicate a substantial stellar population with cosmological age in either the main body or its C component. They suggest instead that I Zw 18 formed coevally or successively within the last $\lesssim$0.5 Gyr.

From the above considerations, we suggest that at least the two following conditions have to be fulfilled for a BCD to be a young galaxy candidate. It must have: a) a single-burst stellar age of the order of the sound crossing time in its warm gas; and b) lack the photometric signatures of a red and uniformly distributed stellar population down to a very faint surface brightness level (e.g. $\sim$29 B mag/$\Box''$). The first criterion is consistent with the hypothesis that the formation of the stellar population dominating the light is due to a single triggering signal propagating through the gaseous halo. The diameter of the LSB* component of I Zw 18 being $\sim$1.3 kpc, corresponds to a timescale of $\sim$130 Myr, assuming a sound velocity in its warm ISM of $\sim$10 km s^{-1} (approximately the HI velocity dispersion in I Zw 18 (van Zee et al. 1998b) and in other dwarf galaxies (cf. e.g. van Zee et al. 1998a; Walter & Brinks 1999; Ott et al. 2001)). This timescale is close to the stellar age estimated above for region ω, assuming an instantaneous burst. The second criterion ensures that an old extended stellar component is either absent or dynamically insignificant. This condition is consistent with the notion that young stars had not yet time to diffuse far enough from their initial locus to gradually form an LSB envelope.

Stellar diffusion, together with propagating star formation (see Noeske et al. 2000 and references therein), may play a key role in the build-up of the LSB component of BCDs. This is suggested by the recent CMD study of the relatively unevolved ($\leq$2 Gyr) *cometary* BCD UGC 4483 (Izotov & Thuan 2002). The main sequence stars in this system are spatially confined to the SF region, while those with progressively larger ages (red supergiants and red giant branch stars) are distributed more evenly and occupy successively larger volumes of the galaxy. This suggests stellar diffusion of young stars to the periphery (Izotov & Thuan 2002). As noted by Izotov & Thuan (2002), the fact that red point sources in I Zw 18 still share the same volume with the young stellar component suggests that these stars have not had time to diffuse out, and that I Zw 18 is considerably younger than UGC 4483.

A study of the role of stellar diffusion on the build-up and structural evolution of the LSB component of dwarf galaxies is beyond the scope of this paper. Nevertheless, it is worth noting that, if this process is primarily driving the formation of the stellar LSB host in young BCDs, then the stars observed in the outermost regions of these systems cannot be younger than a diffusion timescale $\tau_{\rm diff}$. Since at constant diffusion velocity the maximal galactocentric radius that a star can reach scales with the –2.5 power of its mass, stellar diffusion acts as a "mass filter", preventing stars with a lifetime shorter than $\tau_{\rm diff}$ from contributing to the light of the LSB outer regions. In that case, interpreting the colours of the latter assuming continuous SF lasting until the present would result in a systematic age overestimate. The maximum stellar age, as inferred from continuous SF models assuming no SF since a time span $\tau_{\rm diff}$ or instantaneous burst models at various positions along the outermost parts of the LSB host may be a more reliable indicator of the evolutionary state of young BCD candidates. Thus, the estimated single-burst stellar age of $\sim$100 Myr for region ω may be representative for all the LSB* population of I Zw 18, making the BCD an excellent candidate for being a truly young galaxy.

6. Summary and conclusions

The central question to this study is (i) the evolutionary state of I Zw 18 and (ii) whether this galaxy is qualitatively different as compared to standard blue compact dwarf (BCD) galaxies concerning its photometric structure.

We first discuss the photometric structure of two nearby bona fide old BCDs, Mkn 178 and VII Zw 403, to provide a comparison basis for I Zw 18. Both galaxies exemplify that star formation in BCDs does not extend out to a fortuitous galactocentric distance but, as consistently implied by surface photometry and CMD studies, occurs within the 25 B mag/$\Box''$ isophotal radius E_{25} of the underlying low-surface-brightness (LSB) host. The confinement of star-forming activity to the inner part of a BCD results in an appreciable colour contrast ($\sim$0.6–1 $B-R$ mag) between the star-forming and LSB component.

Using ground-based B, V, R, I and J and archival *HST*/WFPC2 images we investigate next the photometric structure of I Zw 18. Our surface brightness profiles (SBPs) confirm the exponential intensity fall-off and the moderately red $B-R$ colour ($\sim$0.6 mag) found in the outer parts of I Zw 18 by Kunth & Östlin (2000) which led them to conclude that I Zw 18 possesses an evolved ($\sim$5 Gyr) and spatially extended stellar disc underlying its star-forming regions.

While the B and R SBPs alone suggest prima facie that I Zw 18 resembles most other BCDs in having an underlying old stellar population, inspection of more colours severely challenges this interpretation. The moderately red $B-R$ colour of the LSB envelope cannot be reconciled with the red $V-R$ (>0.4 mag) and is in conflict with the blue $V-I\sim 0$ mag, $B-V\sim 0.1$ mag and $B-J\sim 0.6$ mag. No evolved population model is consistent with these colours, irrespective of star formation history, age or metallicity. This inconsistency can be removed by taking into account strong contamination of the optical light over galactocentric distances as large as $\sim$1.3 kpc by ionized gas emission. This procedure is further supported by the large (>1300 Å) Hα equivalent widths observed in the periphery of the BCD, as well as by the good spatial correlation of the large Hα equivalent widths with $V-R$ and $V-I$ colours.

We have used archival *HST* narrow-band [O III] λ5007 and Hα images to correct broad-band B, V and R *HST*/WFPC2 images for nebular line emission. While complete removal of ionized gas continuum and line emission is not possible with the available narrow-band images, subtraction of the most prominent nebular emission lines is sufficient to allow us to explore the hypothesis of a stellar host galaxy in I Zw 18. We find that ionized gas contributes $\gtrsim$30% to 50% of the R emission of I Zw 18. The stellar and ionized gas continuum emission dominates the R light only within the effective radius ($R^*\approx 0.2$ kpc), whereas its line-of-sight contribution

decreases to <20% at a galactocentric radius $R^* > 0.65$ kpc. Consequently, the exponential intensity decrease derived in the LSB outer parts ($0.6 \lesssim R^*$ (kpc) $\lesssim 1.3$) of I Zw 18 from uncorrected broad-band images is mainly due to ionized gas emission.

Subtraction of nebular line emission reveals a relatively smooth and very blue stellar LSB envelope (denoted LSB*), extending not much beyond the star-forming regions of I Zw 18. Although our surface photometry does not go below ~26 B mag/$\Box''$, it does allow for a quantitative study of the structural properties and colours of this underlying host galaxy. We find that the latter is not exceptional when compared to intrinsically faint ultra-compact dwarfs, regarding its central surface brightness ($\mu_{\rm E,0} = 20.7$ B mag/$\Box''$) and exponential scale length ($\alpha \approx 120$ pc). This is also the case for I Zw 18 C, which shows in its outer parts an exponential intensity decrease with $\alpha \approx 100$ pc and a marked flattening with respect to the exponential fit for $R^* \lesssim 0.3$ kpc.

Although it does not stand out in the $\mu_{\rm E,0} - \alpha$ parameter space, the LSB* host of I Zw 18, being blue on a radius range of ~5 exponential scale lengths and showing little colour contrast to the star-forming regions, differs strikingly from the underlying component in standard BCDs. The colours, as determined at its southeastern tip where ionized gas emission is negligible, are consistent with an instantaneous burst or continuous star formation starting less than 0.5 Gyr ago. Since I Zw 18 C shows comparably blue colours at its reddest northwestern tip, we conclude that most of the stellar mass in I Zw 18 has formed within the last 0.5 Gyr.

Finally, we show that the exponential intensity decrease observed in the filamentary envelope of I Zw 18 is typical of ionized gaseous halos in star-forming dwarf galaxies. I Zw 18 is not exceptional among BCDs, neither by the extent nor the exponential scale length of its ionized envelope. However, in the absence of a significant underlying stellar population, extended ionized gas emission dominates the light in the periphery of I Zw 18, mimicking the SBP of a relatively red ($B - R \sim 0.6$ mag) old stellar disc.

Acknowledgements. We thank L.-M. Cairós for making available to us Hα images of her BCD sample. Leslie Hunt graciously communicated to us her NIR results on I Zw 18 in advance of publication. We are indebted to the referee, Dr. K. O'Neil, for her comments which helped clarifying the paper. Research by P.P. and K.J.F. has been supported by the Deutsches Zentrum für Luft– und Raumfahrt e.V. (DLR) under grant 50 OR 9907 7. Y.I.I. and N.G.G. have been partially supported by INTAS 97-0033 and Swiss SCOPE 7UKPJ62178 grants. K.G.N. acknowledges the support of DFG grant FR325/50-1. Y.I.I. acknowledges the Göttingen Academy of Sciences for a Gauss professorship and N.G.G. has been supported by the Deutsche Forschungsgemeinschaft (DFG) grant 436 UKR 17/14/01. Those authors acknowledge support by the Volkswagen Foundation under grant No. I/72919. Y.I.I. and T.X.T have been partially supported by NSF grant AST-9616863. T.X.T. also acknowledges the support of *HST* grant GO-08769.01-A. This research has made use of data acquired with the European Southern Observatory telescopes, and obtained from the ESO/ST-ECF Science Archive Facility and of the NASA/IPAC Extragalactic Database (NED) which is operated by the Jet Propulsion Laboratory, CALTECH, under contract with the National Aeronautic and Space Administration.

References

Aloisi, A., Tosi, M., & Greggio, L. 1999, AJ, 118, 302
Aloisi, A., Clampin, M., Diolaiti, E., et al. 2001, AJ, 121, 1425
Beck, S. C., & Kovo, O. 1999, AJ, 117, 190
Binggeli, B., & Cameron, L. M. 1991, A&A, 252, 27
Binggeli, B., & Cameron, L. M. 1993, A&AS, 98, 297
Bomans, D. J. 2002, in Dwarf Galaxies and their Environment, ed. K. S. de Boer, R.-J. Dettmar, & U. Klein (Shaker Verlag), 145
Bothun, G. D., Impey, C. D., & Malin, D. F. 1991, ApJ, 376, 404
Cairós, L. M., Vílchez, J. M., Gónzalez-Pérez, J. N., Iglesias-Páramo, J., & Caon, N. 2001a, ApJS, 133, 321
Cairós, L. M., Caon, N., Vílchez, J. M., Gónzalez-Pérez, J. N., & Muñoz-Tuñón, C. 2001b, ApJS, 136, 393
Cairós, L. M., Caon, N., García Lorenzo, B., Vílchez, J. M., & Muñoz-Tuñón, C. 2002, ApJ, in press [astro-ph/0204343]
Caldwell, N., & Bothun, G. D. 1987, AJ, 94, 1126
Caldwell, N., Armandroff, T. E., Seitzer, P., & Da Costa, G. S. 1992, AJ, 103, 840
Cannon, J. M., Skillman, E. D., Garnett, D. R., & Dufour, R. J. 2002, ApJ, 565, 931
Caon, N., Capaccioli, M., & D'Onofrio, M. 1993, MNRAS, 265, 1013
Carignan, C., & Beaulieu, S. 1989, ApJ, 347, 760
Cellone, S. A., Forte, J. C., & Geisler, D. 1994, ApJS, 93, 397
Chitre, A., & Joshi, U. C. 1999, A&AS, 139, 105
Chitre, A., & Joshi, U. C. 2001, JApA, 22, 155
Christian, C. A., Adams, M., Barnes, J. V., et al. 1985, PASP, 97, 363
Crone, M. M., Schulte-Ladbeck, R. E., Greggio, L., & Hopp, U. 2002, ApJ, 567, 258
Davidson, K., Kinman, T. D., & Friedman, S. D. 1989, AJ, 97, 1591
Doublier, V., Comte, G., Petrosian, A., Surace, C., & Turatto, M. 1997, A&AS, 124, 405
Doublier, V., Caulet, A., & Comte, G. 1999, A&AS, 138, 213
Drinkwater, M., & Hardy, E. 1991, AJ, 101, 94
Drinkwater, M. J., Gregg, M. D., Holman, B. A., & Brown, M. J. I. 2001, MNRAS, 326, 1076
Dufour, R. J., & Hester, J. J. 1990, ApJ, 350, 149
Dufour, R. J., Esteban, C., & Castañeda, H. O. 1996a, ApJ, 471, L87
Dufour, R. J., Garnett, D. R., Skillman, E. D., & Shields, G. A. 1996b, in From Stars To Galaxies, ed. C. Leitherer, U. Fritze-v. Alvensleben, & J. Huchra, ASP Conf. Ser., 98, 358
Fioc, M., & Rocca-Volmerange, B. 1997, A&A, 326, 950
French, H. B. 1980, ApJ, 240, 41
Fricke, K. J., Izotov, Y. I., Papaderos, P., Guseva, N. G., & Thuan, T. X. 2001, AJ, 121, 169
Gil de Paz, A., Zamorano, J., Gallego, J., & de B. Domínguez, F. 2000, A&AS, 145, 377
González-Riestra, R., Rego, M., & Zamorano, J. 1988, A&A, 202, 27
Grebel, E. K. 2001, in Dwarf Galaxies and their Environment, ed. K. S. de Boer, R.-J. Dettmar, & U. Klein (Shaker Verlag), 45
Guseva, N. G., Izotov, Y. I., & Thuan, T. X. 2000, ApJ, 531, 776
Guseva, N. G., Izotov, Y. I., Papaderos, P., et al. 2001, A&A, 378, 756
Heller, A. B., Brosch, N., Almoznino, E., van Zee, L., & Salzer, J. J. 2000, MNRAS, 316, 569
Heydari-Malayeri, M., Melnick, J., & Martin, J.-M. 1990, A&A, 234, 99
Hidalgo-Gamez, A. M., Masegosa, J., & Olofsson, K. 2001, A&A, 369, 797
Hilker, M., Infante, L., Vieira, G., Kissler-Patig, M., & Richtler, T. 1999, A&AS, 134, 75
Holtzman, J. A., Burrows, C. J., Casertano, S., et al. 1995, PASP, 107, 1065
Hopp, U., & Schulte–Ladbeck, R. E. 1991, A&A, 248, 1
Hopp, U., Engels, D., Green, R. F., et al. 2000, A&AS, 142, 417

Hunt, L. K., Mannucci, F., Testi, L., et al. 1998, AJ, 115, 2594
Hunt, L. K., Thuan, T. X., & Izotov, Y. I. 2002, ApJ, submitted
Hunter, D. A., & Thronson, H. A. Jr. 1995, ApJ, 452, 238
Hunter, D. A., Elmegreen, B. G., & Baker, A. L. 1998, ApJ, 493, 595
Izotov, Y. I., & Thuan, T. X. 1998a, ApJ, 497, 227
Izotov, Y. I., & Thuan, T. X. 1998b, ApJ, 500, 188
Izotov, Y. I., & Thuan, T. X. 2002, ApJ, 567, 875
Izotov, Y. I., Lipovetsky, V. A., Chaffee, F. H., et al. 1997, ApJ, 476, 698
Izotov, Y. I., Chaffee, F. H., Foltz, C. B., et al. 1999, ApJ, 527, 757
Izotov, Y. I., Chaffee, F. H., Foltz, C. B., et al. 2001a, ApJ, 560, 222
Izotov, Y. I., Chaffee, F. H., & Schaerer, D. 2001b, A&A, 378, L45
Kennicutt, R. C. 1984, ApJ, 287, 116
Kinman, T. D., & Davidson, K. 1981, ApJ, 243, 127
Kniazev, A. Y., Pustilnik, S. A., Masegosa, J., et al. 2000, A&A, 357, 101
Krüger, H. 1992, Ph.D., Univ. Göttingen
Krüger, H., Fritze-v. Alvensleben, U., & Loose, H.-H. 1995, A&A, 303, 41
Kunth, D., & Östlin, G. 2000, A&A Rev., 10, 1
Kunth, D., Maurogordato, S., & Vigroux, L. 1988, A&A, 204, 10
Landolt, A. U. 1992, AJ, 104, 340
Legrand, F. 2000, A&A, 354, 504
Legrand, F., Kunth, D., Roy, J.-R., Mas-Hesse, J. M., & Walsh, J. R. 2000, A&A, 355, 891
Lequeux, J., Rayo, J. F., Serrano, A., Peimbert, M., & Torres-Peimbert, S. 1979, A&A, 80, 155
Loose, H.-H., & Thuan, T. X. 1986, in Star Forming Dwarf Galaxies and Related Objects, ed. D. Kunth, T. X. Thuan, & J. T. T. Van (Éditions Frontières), 73 (LT86)
Lynds, R., Tolstoy, E., O'Neil, E. J. Jr., & Hunter, D. A. 1998, AJ, 116, 146
Makarova, L. 1999, A&AS, 139, 491
Marlowe, A. T., Meurer, G. R., Heckman, T. M., & Schommer, R. 1997, ApJS, 112, 285
Marlowe, A. T., Meurer, G. R., & Heckman, T. M. 1999, ApJ, 522, 183
Martin, C. L. 1996, ApJ, 465, 680
Mas-Hesse, J. M., & Kunth, D. 1999, A&A, 349, 765
Meurer, G. R., Freeman, K. C., Dopita, M. A., & Cacciari, C. 1992, AJ, 103, 60
Meurer, G. R., Staveley-Smith, L., & Killeen, N. E. B. 1998, MNRAS, 300, 705
Noeske, K. G. 1999, Diploma Thesis, Universität Göttingen
Noeske, K. G., Guseva, N. G., Fricke, K. J., et al. 2000, A&A, 361, 33
Noeske, K. G., Iglesias-Páramo, J., Vílchez, J. M., Papaderos, P., & Fricke, K. J. 2001, A&A, 371, 806
Noeske, K. G., et al. 2002, in prep.
Noguchi, M. 2001, ApJ, 555, 289
Östlin, G. 2000, ApJ, 535, 99
Östlin, G., Bergvall, N., & Rönnback, J. 1996, in The Interplay Between Massive Star Formation, the ISM and Galaxy Formation, ed. D. Kunth, B. Guiderdoni, M. Heydari-Malayeri, & T. X. Thuan (Gif-sur-Yvette: Édition Frontières), 605
Ott, J., Walter, F., Brinks, E., van Dyk, S. D., Dirsch, B., & Klein, U. 2001, AJ, 122, 3070
Pagel, B. E. J., Simonson, E. A., Terlevich, R. J., & Edmunds, M. G. 1992, MNRAS, 255, 325
Papaderos, P., & Fricke, K. J. 1999, in Highlights in X-ray Astronomy, ed. B. Aschenbach, & M. J. Freyberg, MPE Rep., 272, 193
Papaderos, P., Loose, H.-H., Thuan, T. X., & Fricke, K. J. 1996a, A&AS, 120, 207 (P96a)
Papaderos, P., Loose, H.-H., Fricke, K. J., & Thuan, T. X. 1996b, A&A, 314, 59
Papaderos, P., Izotov, Y. I., Fricke, K. J., Thuan, T. X., & Guseva, N. G. 1998, A&A, 338, 43
Papaderos, P., Izotov, Y. I., Noeske, K. G., Thuan, T. X., & Fricke, K. J. 2001, in Dwarf Galaxies and their Environment, ed. K. S. de Boer, R.-J. Dettmar, & U. Klein (Shaker Verlag), 111
Patterson, R. J., & Thuan, T. X. 1996, ApJS, 107, 103
Petrosian, A. R., Boulesteix, J., Comte, G., Kunth, D., & LeCoarer, E. 1997, A&A, 318, 390
Phillipps, S., Drinkwater, M. J., Gregg, M. D., & Jones, J. B. 2001, ApJ, 560, 201
Popescu, C. C., Hopp, U., & Rosa, R. 1999, A&A, 350, 414
Pustilnik, S. A., Kniazev, A. Y., Lipovetsky, V. A., & Ugryumov, A. V. 2001, A&A, 373, 24
Rieschick, A., & Hensler, G. 2000, in 3rd Guillermo Haro Astrophysics Conf., Cosmic Evolution and Galaxy Formation: Structure, Interactions, and Feedback, ed. J. Franco, L. Terlevich, O. López-Cruz, & I. Aretxaga, ASP Conf. Proc., 215, 130
Roye, E. W., & Hunter, D. A. 2000, ApJ, 119, 1145
Rozas, M., Castañeda, H. O., & Beckman, J. E. 1998, A&A, 330, 873
Salzer, J. J., MacAlpine, G. M., & Boroson, T. A. 1989, ApJS, 70, 447
Sargent, W. L. W., & Searle, L. 1970, ApJ, 162, L155
Schulte-Ladbeck, R. E., & Hopp, U. 1998, AJ, 116, 2886
Schulte-Ladbeck, R. E., Crone, M. M., & Hopp, U. 1998, ApJ, 493, L23
Schulte-Ladbeck, R. E., Hopp, U., Crone, M. M., & Greggio, L. 1999a, ApJ, 525, 709
Schulte-Ladbeck, R. E., Hopp, U., Greggio, L., & Crone, M. M. 1999b, AJ, 118, 2705
Schulte-Ladbeck, R. E., Hopp, U., Greggio, L., & Crone, M. M. 2000, AJ, 120, 1713
Searle, L., & Sargent, W. L. W. 1972, ApJ, 173, 25
Sérsic, J. L. 1968, Atlas de Galaxias Australes (Córdoba: Obs. Astron.)
Skillman, E. D., & Kennicutt, R. C. Jr. 1993, ApJ, 411, 655
Smoker, J. V., Axon, D. J., & Davies, R. D. 1999, A&A, 341, 725
Telles, E., Melnick, J., & Terlevich, R. 1997, MNRAS, 288, 78
Terlevich, R., Melnick, J., Masegosa, J., Moles, M., & Copetti, M. V. F. 1991, A&AS, 91, 285
Thuan, T. X. 1991, in Massive Stars in Starbursts, ed. C. Leitherer, N. R. Walborn, T. M. Heckman, & C. A. Norman (Cambridge University Press), 183
Thuan, T. X., Izotov, Y. I., & Lipovetsky, V. A. 1995, ApJ, 445, 108
Thuan, T. X., Izotov, Y. I., & Lipovetsky, V. A. 1997, ApJ, 477, 661
Thuan, T. X., Izotov, Y. I., & Foltz, C. B. 1999, ApJ, 525, 105
Tosi, M., Sabbi, E., Bellazzini, M., et al. 2001, AJ, 122, 1271
van Zee, L. 2000, AJ, 119, 2757
van Zee, L. 2001, AJ, 121, 2003
van Zee, L., Skillman, E. D., & Salzer, J. J. 1998a, AJ, 116, 1186
van Zee, L., Westphahl, D., Haynes, M., & Salzer, J. J. 1998b, AJ, 115, 1000
Vanzi, L., Hunt, L. K., Thuan, T. X., & Izotov, Y. I. 2000, A&A, 363, 493
Vennik, J., Hopp, U., Kovachev, B., Kuhn, B., & Elsässer, H. 1996, A&AS, 117, 261
Vennik, J., Hopp, U., & Popescu, C. C. 2000, A&AS, 142, 399
Viallefond, F., Lequeux, J., & Comte, C. 1987, in Starbursts and Galaxy Evolution, ed. T. X. Thuan, T. Montmerle, & J. Tran Thanh (Éditions Frontières), 139
Vigroux, L., Thuan, T. X., Vader, J. P., & Lachièze–Rey, M. 1986, AJ, 91, 70
Vílchez, J. M. 1995, AJ, 110, 1090
Vílchez, J. M., & Iglesias-Páramo J. 1998, ApJ, 508, 248
Walter, F., & Brinks, E. 1999, AJ, 118, 273
Youngblood, A. J., & Hunter, D. A. 1999, ApJ, 519, 55
Zwicky, F. 1966, ApJ, 143, 192